RESEARCH ARTICLE

Global Change Biology WILEY

Cryptophytes: An emerging algal group in the rapidly changing Antarctic Peninsula marine environments

Carlos Rafael Borges Mendes[1,2] | Raul Rodrigo Costa[1,2] | Afonso Ferreira[1,3] |
Bruno Jesus[4] | Virginia Maria Tavano[1,2] | Tiago Segabinazzi Dotto[5] |
Miguel Costa Leal[6] | Rodrigo Kerr[2] | Carolina Antuarte Islabão[1] |
Andréa de Oliveira da Rocha Franco[1] | Mauricio M. Mata[2] | Carlos Alberto Eiras Garcia[2] |
Eduardo Resende Secchi[7]

[1]Laboratório de Fitoplâncton e Microorganismos Marinhos, Instituto de Oceanografia, Universidade Federal do Rio Grande (FURG), Rio Grande do Sul, Rio Grande, Brazil

[2]Laboratório de Estudo dos Oceanos e Clima, Instituto de Oceanografia, Universidade Federal do Rio Grande (FURG), Rio Grande do Sul, Rio Grande, Brazil

[3]Faculdade de Ciências, MARE – Centro de Ciências do Mar e do Ambiente, Universidade de Lisboa, Lisboa, Portugal

[4]Laboratoire Mer Mólecules Santé, Faculté des Sciences et des Techniques, Université de Nantes, Nantes, France

[5]Centre for Ocean and Atmospheric Sciences, School of Environmental Sciences, University of East Anglia, Norwich, UK

[6]Departamento de Biologia, ECOMARE, CESAM - Centre for Environmental and Marine Studies, Universidade de Aveiro, Aveiro, Portugal

[7]Laboratório de Ecologia e Conservação da Megafauna Marinha, Instituto de Oceanografia, Universidade Federal do Rio Grande (FURG), Rio Grande do Sul, Rio Grande, Brazil

Correspondence
Carlos Rafael Borges Mendes, Laboratório de Fitoplâncton e Microorganismos Marinhos, Instituto de Oceanografia, Universidade Federal do Rio Grande (FURG), Av. Itália, km 8, Rio Grande, RS 96203-900, Brazil.
Email: crbmendes@gmail.com

Abstract

The western Antarctic Peninsula (WAP) is a climatically sensitive region where foundational changes at the basis of the food web have been recorded; cryptophytes are gradually outgrowing diatoms together with a decreased size spectrum of the phytoplankton community. Based on a 11-year (2008–2018) in-situ dataset, we demonstrate a strong coupling between biomass accumulation of cryptophytes, summer upper ocean stability, and the mixed layer depth. Our results shed light on the environmental conditions favoring the cryptophyte success in coastal regions of the WAP, especially during situations of shallower mixed layers associated with lower diatom biomass, which evidences a clear competition or niche segregation between diatoms and cryptophytes. We also unravel the cryptophyte photo-physiological niche by exploring its capacity to thrive under high light stress normally found in confined stratified upper layers. Such conditions are becoming more frequent in the Antarctic coastal waters and will likely have significant future implications at various levels of the marine food web. The competitive advantage of cryptophytes in environments with significant light level fluctuations was supported by laboratory experiments that revealed a high flexibility of cryptophytes to grow in different light conditions driven by a fast photo-regulating response. All tested physiological parameters support the hypothesis that cryptophytes are highly flexible regarding their growing light conditions and extremely efficient in rapidly photo-regulating changes to environmental light levels. This plasticity would give them a competitive advantage in exploiting an

ecological niche where light levels fluctuate quickly. These findings provide new insights on niche separation between diatoms and cryptophytes, which is vital for a thorough understanding of the WAP marine ecosystem.

1 | INTRODUCTION

The local processes of the Southern Ocean have a global impact regulating the Earth's climate (Rintoul, 2018). Like other ocean basins, the Southern Ocean is changing rapidly, with regional differences in the magnitude and direction of such changes (Ferreira et al., 2020; Petrou et al., 2016). These environmental changes have been particularly pronounced in the western Antarctic Peninsula (WAP), which is one of the world's most sensitive regions to climate change (e.g., Steig et al., 2009; Turner et al., 2005), particularly due to a significant sea ice decrease and rapid winter warming over the last decades (Ducklow et al., 2013; Henley et al., 2019; Saba et al., 2014; Stammerjohn et al., 2012). The WAP is unique amongst Antarctic regions due to its NE–SW geographic orientation and direct exposure to prevailing westerly winds and oceanic circulation (Ducklow et al., 2013). Such coastal orientation produces a strong latitudinal climate gradient in both temperature and sea ice cover, which is characterized by a shorter (longer) ice season and more maritime (continental) conditions in the northern (southern) areas (Ducklow et al., 2013; Montes-Hugo et al., 2009; Stammerjohn et al., 2008). The WAP is also strongly influenced by the El Niño Southern Oscillation (ENSO) and the Southern Annular Mode (SAM), which are the two main climate oscillation patterns that influence environmental variability in the Southern Ocean (Stammerjohn et al., 2008). This spatiotemporal environmental variability, in association with the large-scale climate oscillations, has been driving strong shifts in phytoplankton communities (Mendes et al., 2013; Mendes, Tavano, Dotto, et al., 2018; Montes-Hugo et al., 2009; Schofield et al., 2010), particularly marked by latitudinal gradients associated to the progressive southward warming (Brown et al., 2019; Montes-Hugo et al., 2009).

The southernmost sector of the WAP has been somewhat well studied (e.g., Ducklow et al., 2013; Henley et al., 2019; Schofield et al., 2010). However, there are still many key features of phytoplankton communities along the northern Antarctic Peninsula (NAP) that are not yet understood, mainly those related to the intrinsic elusive relationship between anthropogenic climate change and natural climate variability (Ferreira et al., 2020). This knowledge gap is mainly associated with the short-term duration of ship and/or field sampling periods during each season studies carried out in this northernmost region (Ferreira et al., 2020). Overall, such short-term samplings have shown that the spatial distribution of phytoplankton communities around the Antarctic Peninsula's northernmost regions is complex and affected by several environmental factors,

which likely drive their composition and succession stage (Ferreira et al., 2020 and references therein). A common feature among these surveys is that cryptophytes are gradually outgrowing other phytoplankton groups (e.g., diatoms and *Phaeocystis antarctica*), especially in areas influenced by sea-ice and glacial melting processes (Mendes et al., 2013; Mendes, Tavano, Dotto, et al., 2018; Mendes, Tavano, Kerr, et al., 2018).

The northern Antarctic Peninsula (henceforth referred as NAP; Figure 1) covers a wide range of oceanic and coastal ecosystems with complex hydrographic and biogeochemistry dynamics (Kerr et al., 2018). It ranges from the Anvers Island to the oceanic waters surrounding the northern tip of the Antarctic Peninsula, including the Bransfield and Gerlache Straits (Figure S1). The NAP's vulnerability to climate change has resulted in strong environmental variations along its multiple ecosystems (see Figure 1 for an overview of trends over the past 20 years), inducing different selective pressures on biological communities, including shifts in dominant phytoplankton groups (Mendes et al., 2013; Mendes, Tavano, Dotto, et al., 2018; Moline et al., 2004; Montes-Hugo et al., 2009; Schofield et al., 2017). Namely, in the NAP's western sector, sea surface temperature has been rising significantly, contributing to a decrease in seasonal sea ice extent and duration and to thinner glaciers (Cook et al., 2005, 2016; Henley et al., 2019; Stammerjohn et al., 2008). In addition, in the eastern sector, the sea surface salinity has been decreasing due to the disintegration and thinning of the ice shelves (Paolo et al., 2015; Pritchard et al., 2012). Moreover, although atmospheric warming has already exceeded 1.5°C over the second half of the 20th century (Turner et al., 2005), air temperature trends have markedly reversed over the first two decades of the 21st century in the NAP (see inset in Figure 1; Clem et al., 2020; Oliva et al., 2017; Turner et al., 2016). This reversal is mostly explained by regional wind patterns coupled with an inversion of the Interdecadal Pacific Oscillation (Stammerjohn & Scambos, 2020). All these changes reported in the physical environment along the Antarctic Peninsula, particularly sea ice dynamics, have resulted in major shifts in marine food webs across all trophic levels—from primary producers to top predators (e.g., Ducklow et al., 2007; Mendes, Tavano, Dotto, et al., 2018; Schofield et al., 2010).

It has been widely reported that the shift from diatoms to cryptophyte-dominated phytoplanktonic communities has important consequences to the entire food web and, ultimately, to the entire biome of this ecosystem (Ducklow et al., 2007; Ferreira et al., 2020; Moline et al., 2004; Montes-Hugo et al., 2009). However, the mechanisms driving the success of cryptophytes in Antarctic

FIGURE 1 Map of the northern Antarctic Peninsula (NAP) showing the linear trends of environmental changes over the past 20 years. Linear trends (per year) of summer sea surface temperature (SST; color bar), air temperature (inset plot) and sea surface salinity in the NAP between 1998 and 2018. The black solid and dashed lines correspond to positive or negative trend isolines of surface salinity, respectively. The inset plot presents data collected in the Frei, Marambio and Palmer Antarctic stations (location indicated by red, blue and black stars in the main graph, respectively). [Colour figure can be viewed at wileyonlinelibrary.com]
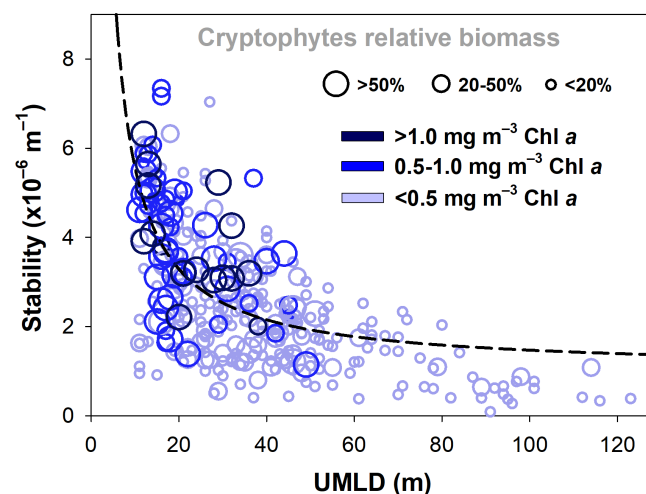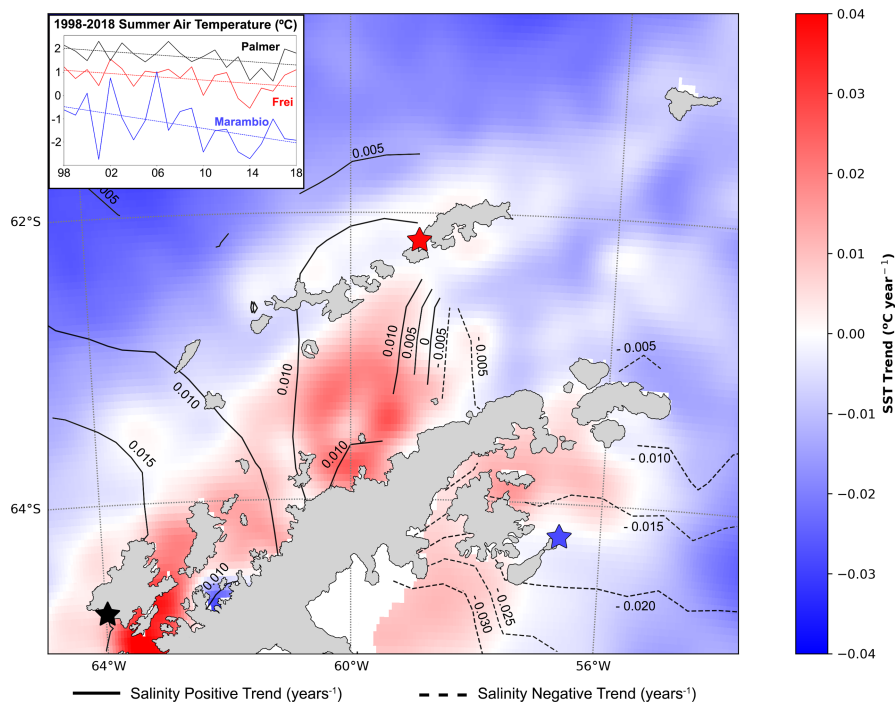
FIGURE 2 Relationship between summer northern Antarctic Peninsula upper ocean physical structure and biomass of cryptophytes. Symbol size indicates the relative contribution of cryptophytes to total chlorophyll *a* (Chl *a*; an index of phytoplankton biomass), whereas symbol color refers to absolute contribution range of cryptophytes . The black dashed line indicates stability modelled as a function of upper mixed layer depth (UMLD; $R^2 = .41$; $p < .0001$; $n = 274$). [Colour figure can be viewed at wileyonlinelibrary.com]

coastal waters are yet to be unraveled. Here, we focus on the rapidly changing NAP using a 11-year (2008–2018) dataset from both the Bransfield and Gerlache Straits (see map of station locations in Figure S1) to demonstrate a strong coupling between summer upper ocean stability, upper mixed layer depth (UMLD) and cryptophytes dominance (Figure 2). We provide particular emphasis on understanding the cryptophyte photo-physiological niche, by exploring its capacity to thrive under high light (HL) stress normally found in

confined stratified upper layers. Such conditions are becoming more frequent in the NAP coastal waters and will likely have significant future implications at various levels of the marine food web, thereby affecting the abundance and availability of key-species such as krill and their predators, and ultimately impacting their fitness and distribution patterns (e.g., Ducklow et al., 2007; Forcada et al., 2006; Nowacek et al., 2011; Seyboth et al., 2016; Trivelpiece et al., 2011).

2 | MATERIALS AND METHODS

2.1 | Oceanographic setting and data collection

Data for this study were collected over 11 years of oceanographic cruises along the NAP, conducted each austral summer (January–February) from 2008 to 2018 onboard the polar vessels *Ary Rongel* (2008–2010) and *Almirante Maximiano* (2013–2018) of the Brazilian Navy. The study area covered the Gerlache Strait, which separates the Anvers and Brabant Islands from the Antarctic Peninsula, and the Bransfield Strait, located between the Southern Shetland Islands and the Antarctic Peninsula (Figure S1). Oceanographic campaigns were not carried out in 2011 and 2012. From 2008 to 2010 the collected data were restricted to the Bransfield Strait. From 2013 onward, data were collected in both the Bransfield and Gerlache Straits (see Table S1 for cruise details). The hydrographic data profiles, such as in situ temperature (°C) and salinity, and seawater discrete samples were collected using a combined Sea-Bird CTD (conductivity–temperature–depth instrument) Carrousel 911+system® equipped with twenty-four 5 L Niskin bottles. Surface seawater samples (from 5 m) were taken in all CTD stations for analysis of phytoplankton pigments. Although

discrete-depth sampling was carried out at some selected stations during the cruises, in this work we only used the information collected at the surface (5 m in depth).

Photosynthetically active radiation (PAR; $\lambda = 400$–700 nm) was measured in the water column (Iz, μmol photons m^{-2} s^{-1}) with a Biospherical Instrument QSP-2300 radiometer attached to the rosette. These data were used to estimate the variability of the light attenuation coefficient (Kd, m^{-1}) at typical stations dominated by cryptophytes and/or diatoms (>50% of total biomass—chlorophyll a). This coefficient was defined by plotting the natural logarithm of the absolute PAR values against their measurement depths and computing the slope of the resulting line. The attenuation profiles revealed minor differences among the sampling stations, with Kd values between 0.11 and 0.16 m^{-1}, highlighting the importance of the UMLD in the light regime to which the phytoplankton is exposed. Unfortunately, PAR measurements along the water column were only available during three cruises. Furthermore, all measurements were performed during daylight stations, between 10:00 and 17:00 h, which were considered appropriate given the prevailing summer solar angle. Stations representative of the presence of cryptophytes and/or diatoms were considered as those with biomass values above 1 mg m^{-3} of chlorophyll a and a relative contribution of cryptophytes or diatoms greater than 50% to the total biomass. Based on this criterion and the daytime measurement restrictions, only 7 (5) stations were representative to cryptophyte (diatom) dominance.

In situ sea surface salinity data (unitless) from 1998 to 2018 was also retrieved from the CORA-GLOBAL in situ Dataset, available in the Copernicus Marine Environment Monitoring Services (CMEMS; https://marine.copernicus.eu/). This dataset integrates data from the main in situ global networks (e.g., Argo, GOSUD, OceanSITES, World Ocean Database). Daily satellite sea surface temperature (°C) with a spatial resolution of 0.05° × 0.05° for the Antarctic Peninsula was extracted from the Operational Sea Surface Temperature and Sea Ice Analysis (OSTIA) product (Good et al., 2020), also available at CMEMS. In situ PAR measurements (μmol photons m^{-2} s^{-1}), collected off the WAP during the U.S. Antarctic Marine Living Resources (AMLR) 2000 cruise (22 February 2000–6 March 2000), were obtained from the NASA SeaWiFS Bio-optical Archive and Storage System (SeaBASS) archive.

2.2 | Water column stability and stratification parameters

Seawater thermodynamic calculations were performed using the Thermodynamic Equation of Seawater–2010 (TEOS-10; McDougall & Barker, 2011). For each CTD cast, the seawater potential density (ρ, kg m^{-3}) referenced to 0 dbar was determined based on seawater conservative temperature, absolute salinity, and pressure data. To examine the water column physical structure, the UMLD (m) and the water column stability ($\times 10^{-6}$ m^{-1}) were calculated from 5 m smoothed profiles of ρ. Although recent studies have estimated

UMLD through the depth of the maximum water column buoyancy frequency (N^2) (Brown et al., 2019; Schofield et al., 2018), this method does not consider the strength of stratification but only the homogeneity of the upper ocean layer. Therefore, to determine the variation of the UMLD based on the strength of stratification, the UMLD was calculated as the depth at which ρ deviates from its 10 m depth value by a threshold of $\Delta\rho = 0.03$ kg m^{-3} (de Boyer Montégut et al., 2004). The water column stability was estimated using vertical ρ variations as a function of N^2 by the local gravity (Costa et al., 2020). To represent the variation of the stability values within the upper ocean layers, the mean stability between 5 and 150 m (upper ocean stability) was used based on the analysis of Costa et al. (2020).

2.3 | High performance liquid chromatography pigment analysis

Phytoplankton pigment analysis was carried on seawater samples (0.5–2.5 L) that were filtered under low vacuum through GF/F filters. The filters were immediately frozen in liquid nitrogen for later high performance liquid chromatography (HPLC) pigment analysis. In the laboratory, the filters were placed in a screw-cap centrifuge tube with 3 mL of 95% cold-buffered methanol (2% ammonium acetate) containing 0.05 mg L^{-1} trans-β-apo-8′-carotenal as internal standard. Samples were then sonicated for 5 min in an ice-water bath, placed at −20°C for 1 h, and then centrifuged at 1100 g for 5 min at 3°C. The supernatants were filtered through Fluoropore polytetrafluoroethylene membrane filters (0.2 μm pore size) to separate the extract from filter remains and cell debris. Immediately prior to injection, 1000 μL of sample was mixed with 400 μL of Milli-Q water in 2.0 mL amber glass sample vials, which were then placed in the HPLC cooling rack (4°C). The pigment extracts were analysed using a Shimadzu HPLC comprised by a solvent distributor module (LC-20AD) with a control system (CBM-20A), a photodiode detector (SPDM20A) and a fluorescence detector (RF-10AXL). The chromatographic separation of the pigments was performed using a monomeric C8 column (SunFire; 15 cm long; 4.6 mm in diameter; 3.5 μm particle size) at a constant temperature of 25°C. The mobile phase (solvent) and respective gradient followed the method developed by Zapata et al. (2000), which was discussed and optimized in Mendes et al. (2007), with a flow rate of 1 mL min^{-1}, injection volume of 100 μL, and 40 min runs. All the studied pigments were identified from both absorbance spectra and retention times, and the concentrations were calculated from the signals in the photodiode array detector in comparison with commercial standards obtained from DHI (Institute for Water and Environment, Denmark). The peaks were integrated using LC-Solution software, and all the peak integrations were checked manually and corrected when necessary. A quality assurance threshold procedure, through application of quantification limit (LOQ) and detection limit (LOD), was applied to the pigment data to reduce the uncertainty of pigments found

—WILEY

in low concentrations (Hooker et al., 2005). The LOQ and LOD procedures were performed according to Mendes et al. (2007). In order to correct for losses and volume changes, the concentrations of the pigments were normalized to the internal standard.

Through HPLC analysis, photo-pigment indices were used to investigate phytoplankton pigment acclimations in response to different environmental light regimes (Mendes, Tavano, Dotto, et al., 2018). The carotenoids were separated into photosynthetic carotenoids (PSCs) and photoprotective carotenoids (PPCs). The PSC included 19′-butanoyloxyfucoxanthin, 19′-hexanoyloxyfucoxanthin, fucoxanthin, prasinoxanthin and peridinin, whereas the PPC were composed by zeaxanthin, violaxanthin, lutein, alloxanthin, diadinoxanthin, diatoxanthin, β,β-carotene and β,ε-carotene (Araujo et al., 2017). Usually, high concentrations of PSCs are associated with high productivity and dominance of large phytoplankton cells, whereas high PPCs proportions indicate a low productivity and dominance of smaller cells, suggesting a potential light stress regime (Mendes et al., 2012; Mendes, Tavano, Dotto, et al., 2018). Therefore, two photo-pigment indices were derived and used here, PSC:Chl-a and PPC:Chl-a. These indices show the proportion of each carotenoid pigment group (PSCs and PPCs) to the total biomass (Chl-a).

The HPLC analysis allows the separation, identification, and quantification of two types of Chl a degradation product: the pheopigments pheophytin a (Phytin a) and pheophorbide a (Phide a). Phytin a is derived from degradation of Chl a by losing the Mg atom, while the Phide a is derived by losing both the Mg atom and the phytol chain, associated with zooplankton gut-related acid exposure (Shuman & Lorenzen, 1975). Pheopigments have long been found in the fecal material of zooplankton (Coelho et al., 2011; Jeffrey, 1974). Thus, the relative content of those degradation products can be used as a proxy for zooplankton assemblage grazing (Costa et al., 2020, 2021; Jeffrey, 1974; Mendes et al., 2012). Hence, the sum of the Phytin a and Phide a was obtained to calculate an index used as a proxy of grazing pressure in this work. This index was computed as the sum of the above phaeopigments divided by a total of Chl a plus degradation products (i.e., sum of Chl a, Phytin a, Phide a and chlorophyllide a), and represented as a percentage.

2.4 | CHEMTAX analysis for determining phytoplankton groups biomass

The absolute and relative contribution of phytoplankton groups to the overall biomass was calculated from the class-specific accessory pigments and total Chl-a using the Chemical taxonomy (CHEMTAX) software v1.95 (Mackey et al., 1996). CHEMTAX uses a factor analysis and steepest descent algorithm to best fit the data onto an initial matrix of pigment ratios (the ratios between the respective accessory pigments and Chl-a). This software package has been extensively and successfully used in many worldwide investigations, including in the Southern Ocean (Brown et al., 2019; Mendes et al., 2012, 2015;

Wright et al., 2010), to determine the distribution and Chl-a biomass of phytoplankton functional groups. This approach provides valuable information about the whole phytoplankton community, including small-size species, which are normally difficult to identify by light microscopy (LM). Although concentration of Chl-a is not an absolute measure of algal biomass, such as carbon, it can be used as a proxy for biomass (Costa et al., 2020; Huot et al., 2007; Jeffrey et al., 1997) since this photosynthetic pigment is common to all autotrophic phytoplankton. Therefore, in this study, we use the term Chl-a referring to either total biomass or relative biomass attributed to the corresponding taxonomic groups. Seven algal groups were selected for CHEMTAX analysis based on previous pigment ratios derived for the NAP (Mendes, Tavano, Kerr, et al., 2018). These groups include diatoms Type-A, diatoms Type-B, dinoflagellates Type-A, dinoflagellates Type-B, cryptophytes, "P. antarctica" and green flagellates. However, in view of the focus of this study, only the absolute and relative biomass of cryptophytes was used, apart from the occasional use of diatom data for comparison purposes.

The whole pigment dataset was separated in two distinct subregions: Gerlache and Bransfield, each of which was separately analysed by CHEMTAX, according to their respective year, to allow for variation in pigment: Chl-a ratios (Mackey et al., 1998). This procedure assured a homogeneity of the pigment: Chl-a ratios within all samples from the same bin, providing some compensation for changes in these ratios, which are known to vary with light availability (Higgins et al., 2011; Schlüter et al., 2000). For optimization of the input matrix, a series of 60 pigment ratio matrices were generated by multiplying each ratio from the initial matrix by a random function as described in Wright et al. (2009). The averages of the best six (10%) output matrices, with the lowest residual or mean square root error, were taken as the optimized results. Lastly, the results of phytoplankton groups derived from the CHEMTAX were quality-controlled by microscopic analysis confirmation.

2.5 | Cryptophyte species isolated from the NAP

Plankton samples containing cells of *Geminigera cryophila* (GEMCRY1) were collected in the Bransfield Strait during the 2016/17 austral summer (25 February 2017; 56.32° W/62.02° S). Cells were isolated, washed and maintained in medium L1 (Guillard & Hargraves, 1993) at salinity (35) and temperature (3±1°C) close to the conditions found in the field, and under white fluorescent light of approximately $100 \mu mol\,photons\,m^{-2}\,s^{-1}$, on 16:8 h light:dark cycle. The L1 culture medium was prepared with seawater collected in the Bransfield region.

2.6 | Experimental setup for the light intensity treatments

To investigate GEMCRY1 growth and photosynthetic characteristics under different light levels, cultures were grown at five

light intensities (3.4, 72, 197, 257 and 535 μmol photons m^{-2} s^{-1}) in a light:dark regime of 14:10 at 3°C for 31 days. The irradiance levels for this experiment were obtained under white light fluorescent lamps (Osram®) and covering the Erlenmeyer flasks with different mesh screens to attenuate light to the intensities mentioned above. Irradiance measurements were made inside the flasks with a submersible Spherical Micro Quantum Sensor (Walz GmbH®). Original cultures were acclimated in each irradiance through at least three transfers over a month during the exponential growth phase. Cells in the early exponential growth phase were inoculated into Erlenmeyer flasks (200 mL, initial densities of 1×10^3 cells mL^{-1}) in triplicate, at each irradiance level. Growth was monitored daily by counting cells in samples fixed with neutral Lugol solution (1%) in Sedgewick Rafter chambers and observed under an inverted microscope at 200× magnification (OLYMPUS IX51). The specific growth rate (μ, day^{-1}) was calculated during the exponential growth phase, when the cell concentrations were log (ln) transformed and a linear regression was applied (Wood et al., 2005; Zar, 1996). Samples for pigment analysis (including phycobiliproteins) were taken after 21 days of culture, which corresponded to the middle-late exponential phase. All experiments were performed in quadruplicate.

2.7 | Pulse amplitude modulation (PAM) fluorescence measurements

To assess the link between photosynthetic light harvesting and photosynthesis PSII quantum efficiency, a second experiment was conducted where GEMCRY1 cells were grown at two constant light intensities (low light [LL] = 35 and HL = 370 μmol photons m^{-2} s^{-1}) in quadruplicate. All fluorescence measurements were made using a pulse-amplitude modulated Phyto-PAM fluorometer (Walz GmbH®). GEMCRY1 photo–physiological parameters were estimated by carrying out rapid light–photosynthesis curve (RLC) responses. The fluorescence parameters estimated from the RLCs were: α, initial slope of the RLC at limiting irradiance; rETRmax, relative unit, maximum relative electron transport rate; Ek = rETRmax/α, μmol photons m^{-2} s^{-1}, light saturation coefficient; and Eopt, μmol photons m^{-2} s^{-1}, optimum light (Eilers & Peeters, 1988). Prior to all RLC, a measurement was carried out on dark adapted sample to measure maximum PSII quantum yields (F_v/F_m). Additionally, both cultures (LL vs. HL) were submitted to a light stress induction and recovery experiment (LSRE), following the same light treatment: 3 min of very LL (14 μmol photons m^{-2} s^{-1}); 9 min of very HL (650 μmol photons m^{-2} s^{-1}); 2 min of very LL (14 μmol photons m^{-2} s^{-1}); and finished by 15 min of darkness. With the LSREs experiments it was possible to determine other physiological parameters such as photosystem II operational quantum efficiency [Y(PSII)] and energy dissipation yield that is not regulated by the cell [Y(NO)]. All fluorescence measurements were made in a stirred, temperature controlled (3°C) chamber. Prior to measurements, all samples were dark adapted in the dark for a minimum of 60 min (Schreiber et al., 1994).

2.8 | Morphometric and phycobilin pigment analysis

For identification purposes, cryptophytes cells were observed and measured using LM ($n = 30$) and scanning electron microscopy (SEM, $n = 10$). Cells were measured and photographed alive under LM at 1000× magnification using a Zeiss Axiocam digital system (ZEISS). Because cryptophytes swimming movements are very fast, the technique to immobilize cells in agarose (Reize & Melkonian, 1989) was also carried out. For SEM analysis, cells were fixed in a 2.5% glutaraldehyde solution, left to settle overnight at room temperature, collected on 1–3 mm pore size nucleopore filters, washed in distilled water, dehydrated through an alcohol series (10%, 25%, 50%, 75% and 100%), and critical-point dried (Cerino & Zingone, 2006). Dried filters were mounted on stubs, coated with gold, and examined under SEM (JEOL JSM−6610 LV; JEOL).

The extraction protocol for phycobiliproteins was carried out according to Thoisen et al. (2017). The cryptophyte samples (10–50 mL each) were concentrated by centrifugation for 10 min at 1100g. The supernatant was decanted, the pellet re-suspended in 3 mL of the extraction solvent 0.1 M phosphate buffer (pH 6.7, 0.05 M K$_2$HPO$_4$, 0.05 M KH$_2$PO$_4$), the slurry homogenized on a vortexer, and frozen at −80°C for 24 h to disrupt the cells. Hereafter, the Falcon® 15 mL conical centrifuge tubes with the pellets were placed in a refrigerator (4°C) for 24 h to complete the extraction process. Then, the extraction mixture was transferred with a plastic Pasteur pipette to a 10 mL syringe with a 25 mm filter (0.2 μm, cellulose acetate membrane), and the filtrate was poured into a 1 cm quartz glass cuvette. The absorbance at 455, 564, 592 and 750 nm was measured on a Shimadzu® UV-2600 spectrophotometer using phosphate buffer as a blank. The measured absorbance values were corrected for light scattering contributions by subtracting the absorbance at 750 nm. The content of phycoerythrin (PE) was calculated according to Beer and Eshel (1985), i.e., PE (mg mL^{-1}) = $[(A_{564} - A_{592}) - (A_{455} - A_{592}) \times 0.2] \times 0.12$; where A refers to absorption at the indicated wavelengths.

Cryptophytes phycobiliproteins are categorized as either a PE (Cr-PE) or phycocyanin (Cr-PC). Cryptophytes with Cr-PE, as is the case of GEMCRY1, generally have pink to red appearance and are divided into three classes according to the wavelength of maximal absorption. The absorption peak of the purified preparation of phycobiliproteins from GEMCRY1 was at 545 nm. Therefore, the GEMCRY1 phycobiliprotein was identified as Cr-PE 545.

2.9 | DNA sequencing and phylogenetic inference

The strain GEMCRY1 DNA was extracted from centrifuged pellets using the DNeasy® Plant Mini Commercial Kit (QIAGEN). The amplification of 18S rDNA was carried out with Platinum® Taq DNA Polymerase (Invitrogen) and the primers CrNIF and Br (Marin et al., 1998) in a thermocycler (The Veriti Dx™ 96-Well Thermal Cycler; Applied Biosystems). The PCR conditions followed recommendations in Marin et al. (1998). The amplified products were

purified with the QiaQuick PCR Purification Kit (QIAGEN). The sequencing was performed with BigDye Terminator v3.1 Cycle Sequencing Kit using the automatic sequencer AB 3500 Genetic Analyzer (Applied Biosystems) by ACTGene Análises Moleculares Ltd. (Center for Biotechnology, UFRGS, Porto Alegre, RS, Brazil). Sequencing reactions were performed with the PCR primers (CrNIF and Br) and additional internal sequencing primers (528>; 920>; 920<; 536<) that were designed by Marin et al. (1998). These internal primers were used only in sequencing reactions to allow overlap between reverse and forward sequences, as used in some taxonomic studies on cryptophytes (Laza-Martínez, 2012; Marin et al., 1998).

The phylogenetic tree was produced with 36 sequences identified at the species level from Genbank representing mainly Cryptophyceae class (Daugbjerg et al., 2018; Laza-Martínez, 2012) plus one sequence of our strain and two sequences of Katablepharid (*Leucocryptos marina* and *Roombia truncata*) as outgroups (Burki et al., 2020). The sequences were aligned using Clustal Omega (Madeira et al., 2019), then the alignment obtained was manually edited and trimmed using MEGA-X software (Kumar et al., 2018), generating a data matrix with 39 sequences (18S rDNA) and 1669 alignable positions. Phylogenetic inferences were based in Bayesian analysis (BA) and maximum likelihood analysis (ML) using a GTR family model with gamma distribution and invariant sites (+G+I) (Rodriguez et al., 1990). This model was selected to be applied to the data matrix using the Akaike information criterion (Akaike, 1974) by the software jModel Test 2 (Darriba et al., 2012). BA was performed with Markov Chain Monte Carlo sampling method in two runs, four chains of 10 million generations each, one topology sampled each 500 generations and a discard of 25%, using the software MrBayes 3.2.3 (Ronquist & Huelsenbeck, 2003). The convergence between runs and analysis performance was validated with the likelihood plots for each run and the effective sample size (>200) using Tracer v.1.7.1. The ML was run using the software MEGA-X and the *bootstrap* were calculated from 5000 replications (Kumar et al., 2018; Nei & Kumar, 2000). The tree topology was based on BA and the robustness of clades were evaluated by probability from BA and *bootstrap from ML*.

3 | RESULTS AND DISCUSSION

3.1 | The distribution, dominance patterns and niche preferences of cryptophytes

Phytoplankton is a diversified group of unicellular photosynthetic organisms, globally important for their role as ocean primary producers and key players in the cycling of carbon and nutrients (Falkowski et al., 1998). Antarctic food webs are sustained by these photosynthetic microorganisms, particularly by large-celled diatoms that usually dominate phytoplankton communities in highly productive Antarctic regions (e.g., Armbrust, 2009; Arrigo et al., 1999; Costa et al., 2020; Pondaven et al., 2000). These large bloom-forming marine microorganisms are responsible for more than 85% of total

annual primary production in the Southern Ocean (Rousseaux & Gregg, 2014). The high phytoplankton productivity in the Antarctic waters, particularly in coastal regions, is fuelled by an abundant supply of nutrients (Kim et al., 2016) and the availability of light when the mixed layers are shallow, thus allowing cells to overcome light limitation (Brown et al., 2019; Costa et al., 2020; Ducklow et al., 2007; Mendes, Tavano, Dotto, et al., 2018; Mendes, Tavano, Kerr, et al., 2018; Schofield et al., 2017).

Latitudinal changes in NAP phytoplankton biomass have been recorded and attributed to regional climate patterns reflected by a progressive warming towards the southern end of the Peninsula, with increasing chlorophyll-*a* in that sector, contrasting with trends recorded northwards (Brown et al., 2019; Montes-Hugo et al., 2009). Moreover, these changes in phytoplankton biomass have been followed by shifts in community composition, particularly resulting in a smaller fraction of large diatoms in the northern sector (Bahlai et al., 2021; Brown et al., 2019; Montes-Hugo et al., 2009; Schofield et al., 2010). In the NAP region, specifically, several studies have reported an increasing contribution of small cryptophytes to the phytoplankton community composition (e.g., Mendes et al., 2013; Mendes, Tavano, Dotto, et al., 2018; Mendes, Tavano, Kerr, et al., 2018), with our decadal in situ dataset suggesting a niche segregation between cryptophytes and diatoms based on physical and chemical properties of the water-column (Figure S2). The variation in upper ocean physical structures caused by the influence of glacial meltwater input (lower-salinity waters), which leads to shallower-stabilized upper layers (Meredith et al., 2021), apparently does not favor the development of diatom bloom (Costa et al., 2021), leaving the well-lit surface waters free for cryptophytes to grow (Figure S2).

Intriguingly, opposite to what might be expected, absolute concentrations of cryptophytes and diatoms are statistically similar at their high proportions, i.e., where either shows >50% biomass (Figure S3), which supports a decreased contribution of large diatom cells accumulation along the NAP (Montes-Hugo et al., 2009). Such potential shifts in phytoplankton size composition affect phytoplankton-grazer relationships with important ecological consequences to the structure and functioning of the Antarctic ecosystem (Ducklow et al., 2007; Saba et al., 2014).

Temperature and salinity are two major environmental factors driving growth, development, and survival of marine planktonic organisms, mainly through changes in seawater density that determine water column stratification, and hence vertical stability (Ferreira et al., 2020; Petrou et al., 2016). However, due to the nonlinear nature of the equation of state of seawater density, the sensitivity to temperature reduces as temperature approaches the freezing point, thereby increasing the importance of salinity as the main environmental variable controlling stratification levels in polar regions (Falkowski et al., 1998). The increasing meltwater input around the Antarctic Peninsula recorded in the last decades due to warmer temperatures has therefore increased the importance of shallower UMLDs and water column stability as key environmental drivers controlling biomass and composition of phytoplankton communities (Brown et al., 2019; Costa et al., 2020; Dierssen et al., 2002;

Höfer et al., 2019; Mendes et al., 2012). In surface Antarctic waters, the abundance of cryptophytes has been frequently associated with low-salinity and highly stable water layers (Brown et al., 2019; Henley et al., 2019; Moline et al., 2004; Rozema et al., 2017; Schofield et al., 2017), in which they thrive by active swimming. These patterns are clearly visible in the NAP, where salinity is the main driver contributing to water column stratification in the region (Figure S4a,c), thus providing the ideal conditions for the development of cryptophytes under less salty waters (Figure S5a). Such conditions are evident in the Gerlache Strait, where average salinity values are typically below 34 (Figure 3a), likely associated with this strait being heavily glaciated by valley glaciers and ice caps (Pan et al., 2020). In the Bransfield Strait, the presence of cryptophytes is more sporadic; however, their greatest contribution to the phytoplankton community composition was also recorded in lower salinity levels, particularly in the years 2010, 2014 and 2017 when average salinity was under 34 (Figure 3b). Seawater temperature, despite having a secondary role in the stratification processes (Figure S4b,d), can enhance water column stabilization and favor the development of

cryptophytes at near surface layers in certain situations or areas of the study region, such as in the Gerlache Strait (Figure S5b; Mendes, Tavano, Dotto, et al., 2018).

The correlation of cryptophytes with stratified conditions along the WAP has been previously reported (e.g., Mendes et al., 2013; Rozema et al., 2017), but the drivers of their emergence and success in Antarctic coastal waters remain unknown (Henley et al., 2019). This is, in part, due to the difficulty in quantifying their physiological responses in situ, and to the knowledge gap in understanding their fundamental biological features, as only a few Antarctic cryptophyte species are available in laboratory cultures. Nevertheless, the strong dominance of cryptophytes in WAP coastal waters has been previously attributed to factors such as the selective grazing (Garibotti et al., 2003), iron scarcity (Mendes et al., 2013), sedimentation of large diatoms (Castro et al., 2002) and/or preference/physiological tolerance of cryptophytes to lower salinity waters (Moline et al., 2004). Based on our results, the top-down control does not seem to play an important role modulating biomass accumulation of cryptophytes in shallower mixing layers (Figure S6). In general, the stations dominated by cryptophytes were associated with lower grazing index values (Figure S6), suggesting a low grazing pressure in areas influenced by glacial melting processes, and associated with cryptophyte dominance. Melting water input could mitigate grazing pressure in lower salinity and stratified waters where cryptophytes prevail, probably associated with melt water dilution. In contrast, the diatom-dominated stations were associated with a greater grazing activity (higher grazing index values) in relatively deeper UMLDs, evidencing an effective top-down control associated with diatom dominance (Figure S6). Cryptophytes appear to occupy the environment that follows local glacier melting, not having to endure competition with other phytoplankton groups for resources (Pan et al., 2020). This suggests that such cryptophyte-dominated system associated with meltwater input is mostly bottom-up controlled. On the other hand, most studies suggest that glaciers, icebergs and freshwater runoff are the main sources of lithogenic material for the region, containing relatively high concentrations of particulate and some dissolved trace metals, especially dissolved iron (e.g., Annett et al., 2015; Mora et al., 1994; Shaw et al., 2011). Therefore, it is unlikely that the observed low diatom biomass accumulation in stratified layers results from a lack of specific micronutrients that could hinder its growth. While sinking may also be a plausible factor affecting large diatoms in stratified shallow mixing layers (Costa et al., 2021), it would only influence their biomass accumulation, not necessarily preventing their growth, depending on the speed of cells sinking.

It has recently been suggested that the gradual dominance of cryptophytes in the well-lit surface layers along NAP coastal waters might be associated with a high tolerance of cryptophytes to relatively high irradiance, due to an optimization of their light-harvesting capability, which increases their photoprotective pigment pool (Mendes, Tavano, Dotto, et al., 2018). A previous study in the Palmer station region—in the southernmost sector of the WAP—had already highlighted this distinct response of cryptophytes regarding their light utilization efficiency as a function of the contribution of
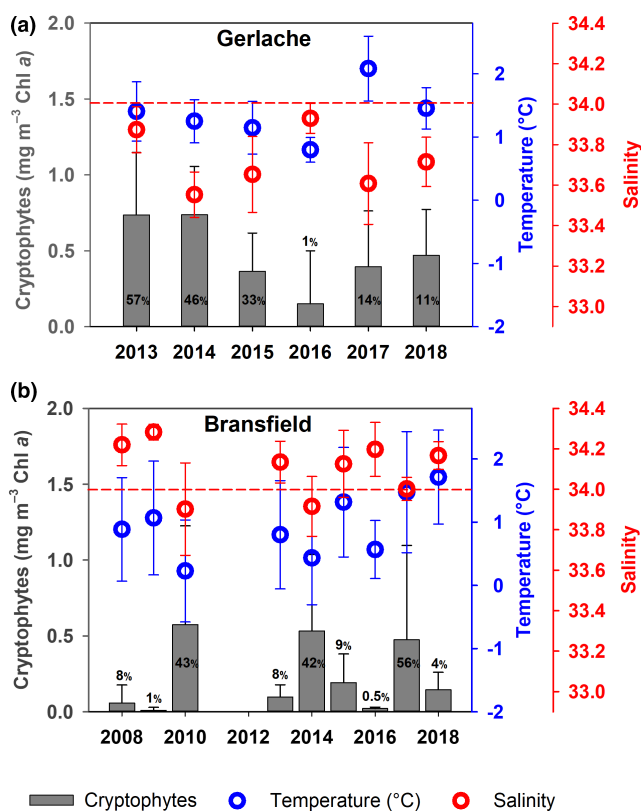
FIGURE 3 Interannual variability of cryptophyte's biomass along the northern Antarctic Peninsula. Mean summer values and standard deviation of absolute contributions (mg m^{-3} Chl a) of cryptophytes, and respective mean sea surface temperature and mean surface salinity values and their standard deviation in the (a) Gerlache and (b) Bransfield Straits. The horizontal red dashed line represents the salinity value of 34. The numbers inside the bars indicate the mean summer relative (%) contributions of cryptophytes (to the total biomass; Chl a). Data were collected during the late summer cruises (see Section 2). [Colour figure can be viewed at wileyonlinelibrary.com]

photoprotective pigments (Claustre et al., 1997). Indeed, using our in-situ pigment database, we observed a direct link between cryptophyte proportion and an increase in the proportion of photoprotective carotenoid pigments (values of PPC:Chl-*a*—the amount of photoprotective pigments to total chlorophyll *a*—between 0.4 and 0.5), while this proportion decreases to ~0.1 in samples dominated by diatoms (Figure S7). Although these results indicate an optimization of light harvesting antenna of cryptophytes to higher-light regimes, ecophysiological studies (both in situ and in vivo) on these organisms are still scarce, and a better characterization of their photosynthetic performance is needed. To fill this gap in current knowledge, we tested in laboratory the effects of irradiance on the photosynthetic physiology of the Antarctic cryptophyte *G. cryophila* isolated from the NAP region during our February 2017 field campaign (see Section 2 for more details). Results (discussed next) revealed that cryptophytes are highly adaptable in photo-regulating their exposure to extreme light transitions, even when cultivated at very LL levels.

3.2 | Taxonomy, pigment composition and photo-physiological plasticity of cryptophytes

The Antarctic cryptophyte used as a model in this work—GEMCRY1—was identified as *G. cryophila* based on its cell morphology, observed by optical microscopy and SEM, pigment content and nuclear 18S rDNA phylogeny (Figure S8a–c). This strain has a morphology (ellipsoid and flattened cells, tapering towards posterior end) and size range (9–13 μm long and 4–8 μm wide) similar to the *G. cryophila* described by van den Hoff et al. (2020), though significantly smaller than the morphological features reported for this same species in earlier studies (Hill, 1991; Taylor & Lee, 1971). However, cells' characteristics reported here are consistent with the original description of *G. cryophila* (Hill, 1991; Taylor & Lee, 1971). Namely, GEMCRY1 contains PE with a maximum absorption of 545 nm (CrPE 545), a single chloroplast, two pyrenoids, a nucleus situated in the posterior end, an extrapyrenoidal nucleomorph and a longitudinal furrow of medium length coated by apparent ejectisomes (Emden et al., 2002; Hill, 1991; Novarino, 2003). The cell surface has a warty appearance (Figure S8b) due to a high accumulation of lipid droplets in the peripheral cytoplasm (Hill, 1991).

Nuclear 18S rDNA tree topology (Figure S8d) agrees, in general, with those previously published, resolving the clades of plastid-containing cryptophytes lineages (Daugbjerg et al., 2018; Deane et al., 2002; Laza-Martínez, 2012). *Cryptomonas* (clade A); *Geminigera/Teleaulax/Plagioselmis* (clade B); *Guilardia/Hanusia* (clade C) *Rhodomonas/Storeatula/Rhinomonas* (clade E); and single-species lineages of *Baffinella frigidus* and *Urgorri complanatus* are highly supported with posterior probability (PP) = 1 and bootstrap (BS) = 100 (Figure S8d). The group *Chroomonas/Komma/Hemiselmis* was not monophyletic in our analysis (Figure S8d); however, these cryptophytes formed a clade with only moderate support in a previous study (Laza-Martínez, 2012). *Falcomomas daucoides* and *Proteomonas*

sulcata formed a clade well supported only by PP = 0.99 and low support at BS = 78, suggesting that this relationship may be found by chance (Figure S8d). The GEMCRY1 strain was included in the clade B and formed a smaller clade with two other *G. cryophila* strains. The *G. cryophila* original description is based on a strain isolated from the Weddell Sea (Hill, 1991; Taylor & Lee, 1971), while GEMCRY1 was isolated from Bransfield Strait. The genetic similarity was high (~99%) between GEMCRY1 and other *G. cryophila* strains from Antarctica available in GenBank: 99.9% (Ace lake: HQ111513.1), 99.3% (McMurdo Sound: DQ452091.1), 99.2% (Weddell Sea: U53124.1), and 99.1% (Bayly Bay: HQ111512.1). These values are consistent with previously obtained genetic similarity between strains of *G. cryophila* (van den Hoff et al., 2020), confirming the identification of GEMCRY1 as *G. cryophila*. Among Cryptophyceae, *G. cryophila* has been one of the main species found in WAP coastal waters, with small contributions of the genera *Hemiselmis* and *Plagioselmis* (Trefault et al., 2021). Confirming the importance of *G. cryophila* in the study region, a recent investigation using a 5-year data set of 18S rRNA revealed that there is a clear dominance of only one cryptophyte taxon belonging to the genus *Geminigera* (average taxon percentage of 96%), which closely matches the *G. cryophila* strain from the Ace Lake (Brown et al., 2021).

Cryptophytes are a cosmopolitan group that thrive in diverse aquatic environments, such as oligotrophic waters (Ilmavirta, 1988), coastal waters (Tamigneaux et al., 1995), estuaries (Pinckney et al., 1998), inland lakes (Higashi & Seki, 2000), and the Southern Ocean (Mendes et al., 2013; Moline et al., 2004). While most cryptophytes are autotrophic, a significant number of mixotrophic species has been described (Davis & Sieburth, 1984; Hill & Rowan, 1989). The mixotrophic nature has been hypothesized as a strategy to permit cells to supplement photosynthesis, allowing them to thrive in dim light conditions, which are found at the depths where they often reside (Bergmann et al., 2004; Ilmavirta, 1988). In fact, although little is known about cryptophyte light-harvesting mechanisms, some studies have suggested that many of these algae are adapted to LL and use quantum coherence to improve the efficiency of energy transfer (Collini et al., 2010; Harrop et al., 2014). Cryptophytes, unlike other chlorophyll-*c* containing (or chromalveolate) microalgae, use both chlorophyll *a/c* proteins and phycobiliproteins (acquired from a red algae symbiotic ancestral) as their light harvesting pigment complex (Cunningham et al., 2019). This combination has allowed them to specialize and diversify within LL environments, where increased light-harvesting capacity is essential (Bergmann et al., 2004; Ilmavirta, 1988). Therefore, it is intriguing that, around the Antarctic Peninsula, the cryptophytes mainly occupy a different niche than in other oceanic regions and are often confined to the shallow well-lit euphotic layers. Their presence in these HL environments would require high photo-regulation capabilities to be able to thrive under the extreme light levels.

To investigate the growth and photosynthetic characteristics of GEMCRY1 under different light levels, cultures were grown under five light intensities (from 3.4 to 535 μmol photons m^{-2} s^{-1}) in a light: dark regime of 14:10 at 3°C for 31 days (see Section 2 for more

details). The cryptophyte GEMCRY1 grew well at all light-intensities, except for the lowest light level of 3.4 μmol photons m^{-2} s^{-1}, where *G. cryophila* was unable to grow, suggesting that this species is not capable of growing at very LL intensities (Figure S9). Similar growth rates were observed in the range between 72 to 535 μmol photons m^{-2} s^{-1} (Figure S9), showing high flexibility for growing in a relatively wide range of light conditions. Although there were no significant changes in growth under different light regimes, GEMCRY1 cells were capable of dynamically adjusting their pigment content in accordance with the ambient light intensity (Figure 4; Figure S10).

All phytoplankton, including cryptophytes, have chlorophyll *a* as their major light-harvesting pigment (Roy et al., 2011). Cryptophytes also use accessory pigments (alloxanthin, α-carotene, chlorophyll *c*$_2$ and phycobiliproteins) to increase the spectral range of light capture (Hill & Rowan, 1989). The ratio of chlorophyll *a* to other pigments varies among cryptophytes and, in many species, the cellular concentration of phycobiliproteins is higher than that of non-phycobiliprotein pigments (Cunningham et al., 2019). This was also seen for GEMCRY1, where PE Cr-545 (CrPE 545) represented between 60% and 70% of the total pigments per cell—depending on light intensity. Currently, there is a scarcity of data on cellular pigment content for the Antarctic cryptophytes, especially those that include phycobiliproteins, chlorophylls and carotenoids together. As an exception, Cunningham et al. (2019) reported cellular CrPE 545 concentrations of 6.6 ± 1.9 pg cell^{-1} for *G. cryophila*, while Chl-*a* for the same strain was 4.2 ± 0.2 pg cell^{-1}. These concentrations are

relatively higher than values observed in this present study (1.5–6.9 pg cell^{-1} for CrPE 545; 0.6–1.7 pg cell^{-1} for Chl-*a*—depending on light exposure), though culture conditions differed, hindering to establish a direct comparison. Most importantly, the results recorded here for GEMCRY1, using different light levels, demonstrate the great plasticity of the Antarctic cryptophyte *G. cryophila* in altering their pigment content, evidencing a clear regulation capacity of photosynthetic light-harvesting pigments to changes in the light regime (Figure 4). At the lowest light intensity (72 μmol photons m^{-2} s^{-1}), cells contained approximately two to three times more total pigments (mainly CrPE 545 and Chl-*a*) than cells acclimated at 197 μmol photons m^{-2} s^{-1}. Between 197 and 535 μmol photons m^{-2} s^{-1}, there was also a decrease of total pigments per cell (from 3.7 to 2.8 pg cell^{-1}), but much less marked than in the first levels of light tested (from 9.6 to 3.7 pg cell^{-1}) (Figure 4). Regarding the effects of irradiance on chlorophyll *a/c* antennae pigments, the alloxanthin in cryptophytes has been recognized as having a photoprotective pigment role (Funk et al., 2011; Laviale & Neveux, 2011). For instance, increase in alloxanthin-to-Chl-*a* ratio (Allo:Chl-*a*) has been observed in cultures of cryptophytes acclimated to HL (e.g., Funk et al., 2011). Accordingly, in our light-related physiology experiment, the Allo:Chl-*a* ratio also increased significantly with increasing light intensities (from 0.3 on 72 μmol photons m^{-2} s^{-1} to 0.7 on 535 μmol photons m^{-2} s^{-1}) (Figure 4). Nevertheless, this increase was more related to the decrease in Chl-*a* content than to the increase in alloxanthin. In fact, the alloxanthin content decreased from 0.56 pg cell^{-1} on 72 μmol photons m^{-2} s^{-1} to 0.35 pg cell^{-1} on 197 μmol photons m^{-2} s^{-1}, followed by a slight increase towards the highest light intensity (from 0.36 pg cell^{-1} on 257 μmol photons m^{-2} s^{-1} to 0.43 pg cell^{-1} on 535 μmol photons m^{-2} s^{-1}) (Figure 4). This apparently paradoxical result in alloxanthin behavior, keeping its concentration relatively stable over all tested light intensities, may be associated with alloxanthin being a light-harvesting carotenoid, transferring energy efficiently to Chl-*a* (West et al., 2016) and playing, simultaneously, an effective role in the photoprotective quenching (Kaňa et al., 2012).

Regulation of photosynthetic light harvesting in the thylakoids and photosynthetic electron transport rate (ETR) is one of the major key factors affecting photosynthetic efficiency. To assess this link, we acclimated GEMCRY1 in a parallel experiment to two different light intensities: 36 and 370 μmol photons m^{-2} s^{-1}, henceforth referred to as LL and HL, respectively. Photosynthesis–irradiance light response curves were carried out to characterize their photo–acclimation status (see Section 2 for more details) showing marked differences between the two conditions, with HL cells having much higher Ek, Eopt, rETRmax values and much lower α values than LL cells (Figure S11), which are classical indicators of HL versus LL acclimation (Ralph & Gademann, 2005). To test the capacity of these cells to cope with sudden light stress we assessed their capacity to change from very LL (14 μmol photons m^{-2} s^{-1}) to HL (650 μmol photons m^{-2} s^{-1}) for 10 min and then measured their recovery in very LL followed by darkness for 20 min. Both cultures started with high F_v/F_m values (>0.65), with a slight decrease of operational PSII quantum yield [Y(II)] when exposed to 14 μmol photons m^{-2} s^{-1}, thus
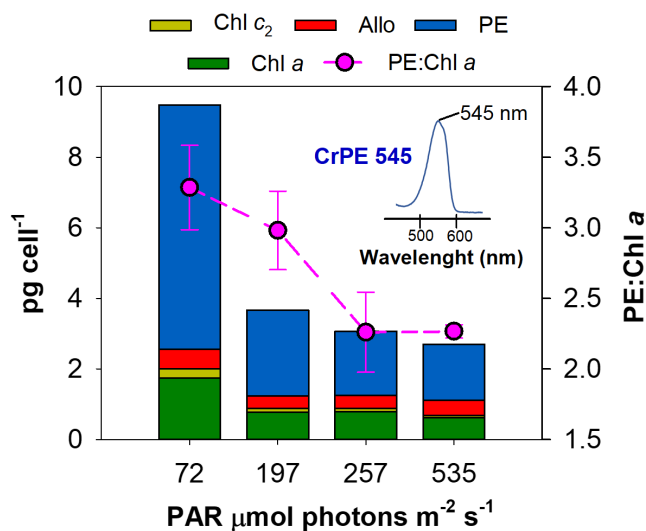
FIGURE 4 Variations in pigment contents of the cryptophyte *Geminigera cryophila* grown under different light regimes. Mean values of pigment concentrations per cell (pg cell^{-1}) of *G. cryophila* acclimated to four different light intensities (72, 197, 257 and 535 μmol photons m^{-2} s^{-1}). Chl *c*$_2$ = chlorophyll *c*$_2$; Allo = alloxanthin; PE = phycoerythrin; Chl *a* = chlorophyll *a*. The ratio PE:Chl *a* is also represented. The concentration of the minor pigments β,ε-carotene and crocoxanthin was residual and thus was not plotted. The inset graph shows the peak of absorbance centered at 545 nm of PE extracted from the cryptophyte GEMCRY1 (*G. cryophila*), referred here to as CrPE 545. [Colour figure can be viewed at wileyonlinelibrary.com]

showing that even the HL cells were capable of using these LLs to carry out ETR. When exposed to 650 μmol photons m^{-2} s^{-1}, the Y(II) of both cultures showed a tri-phasic response, starting with a sharp decrease—reaching zero in LL cells—followed by a quick recovery and a final stage of constant values until the end of the light stress step. Recovery to initial values was almost complete within 5 min of exposure to 14 μmol photons m^{-2} s^{-1} and only a small increase was observed in darkness for the LL cells (Figure 5a). The quick recovery of the LL cells exposed to the stress of 650 μmol photons m^{-2} s^{-1} and the lack of evidence of photo-inhibition shown by the full recovery of F_V/F_m values after 20 min in darkness clearly show that the LL cells were capable 18-times more of sustaining exposure to light than their growing light (36 μmol photons m^{-2} s^{-1}), and recovering very quickly
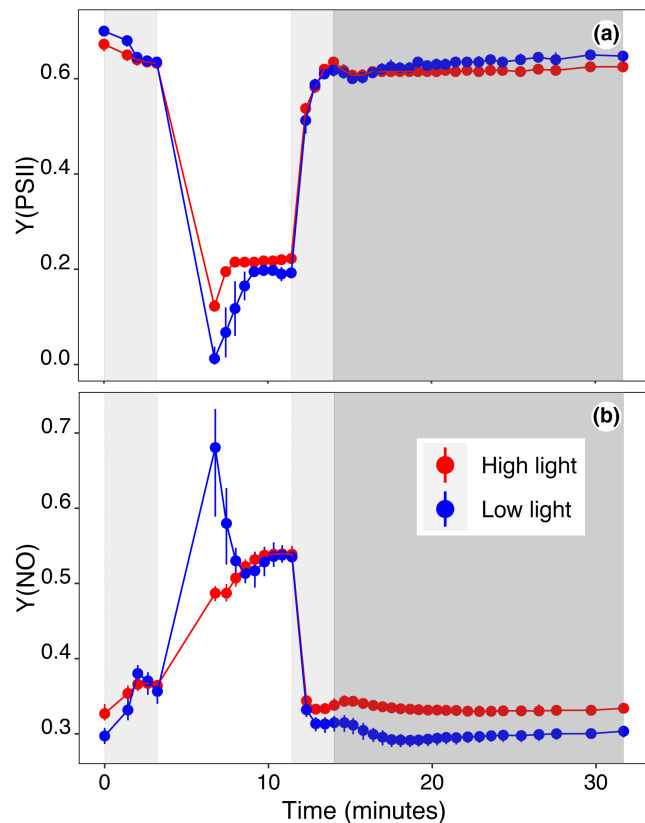
FIGURE 5 Pulse amplitude modulation (PAM) fluorescence variations of *Geminigera cryophila* acclimated to different light regimes; submitted to a light stress induction and recovery experiment. High light cells were acclimated to 370 μmol photons m^{-2} s^{-1} and Low light cells were acclimated to 36 μmol photons m^{-2} s^{-1}. Both cultures were exposed to the same light treatments. Namely: 3 min of very low lights (14 μmol photons m^{-2} s^{-1}); 9 min of very high light (650 μmol photons m^{-2} s^{-1}); 2 min of very low light (14 μmol photons m^{-2} s^{-1}); and finished by 15 min of darkness. Light grey areas correspond to very low light, white area corresponds to very high light and dark grey area corresponds to the darkness recovery period. Each point corresponds to mean values and 95% confidence intervals. (a) Photosystem II operational quantum efficiency [Y(PSII)]. (b) Energy dissipation yield that is not regulated by the cell [Y(NO)], that is, the sum of non-regulated heat dissipation and fluorescence emission. [Colour figure can be viewed at wileyonlinelibrary.com]

(Figure 5a). The stress-recovery experiment also showed that the HL-cells were already capable of carrying out some photochemistry at very LL levels (25 times lower than their growing light). The main difference between the two cultures is their immediate capacity to photo-dissipate energy in a controlled way (Figure 5b). The Y(NO) parameter presented in Figure 5b represents the energy fraction that is dissipated by heat and fluorescence but not linked to regulated photo-protective mechanisms [i.e., Y(NPQ)]. The LL-acclimated cells show a Y(NO) peak not observed in the HL-acclimated cells; however, this peak is quickly (<5 min) reduced to the same level as HL-cells (Figure 5b). In conclusion, all pulse amplitude modulation (PAM) fluorescence parameters support the hypothesis that GEMCRY1 is highly flexible regarding their growing light conditions and extremely efficient in rapidly photo-regulating changes to environmental light levels. This plasticity would give them a competitive advantage in exploring a niche where light levels fluctuate quickly.

3.3 | Photophysiological mechanisms in the upper ocean mixed layer

Light regimes in the Southern Ocean vary dramatically over the course of a season, but the maximum levels of daily integrated irradiance at the ocean surface in summer can be as high as in the tropics (Campbell & Aarup, 1989). However, rapid variations in light (Figure S12) caused by frequent strong winds, which drive deep mixing, and shading by pack sea ice and cloud cover, reduce the effective irradiance levels in the water column. As a result, Antarctic phytoplankton tends to mostly adapt to LL conditions, being able to operate at their maximal photosynthetic capability at light levels corresponding to only a small fraction of incoming irradiance (Dierssen et al., 2002).

Light availability in the water column depends primarily on UMLD (Joy-Warren et al., 2019). While deep mixing moves phytoplankton cells below the physiological compensation depth where primary production is typically limited by light, shallower mixing layers confine planktonic organisms near the surface, exposing them to a complex light regime with fluctuating periods of direct and indirect sunlight (Moreau et al., 2010). The great variability in sunlight levels near the surface may strongly affect phytoplankton establishment and growth (Petrou et al., 2016). However, quantifying the complex light conditions occurring within the mixed layer and relating them to phytoplankton growth is extremely difficult.

Throughout the photoperiod, incident sunlight in the mixed layer is attenuated exponentially with depth. Consequently, the depth of the mixed layer can have a drastic effect upon photosynthetic capacity, as phytoplankton organisms acclimate to their predominant light exposure (Alderkamp et al., 2010). In our study region, the mixed-layer depth was relatively deep at the diatom–dominated sites (~40 m), whereas it ranged between 15 and 20 m in regions with a clear dominance of cryptophytes (Figure 6). This duality has already been reported by other time-constrained studies conducted in the region (Costa et al., 2020; Mendes et al., 2013; Mendes,
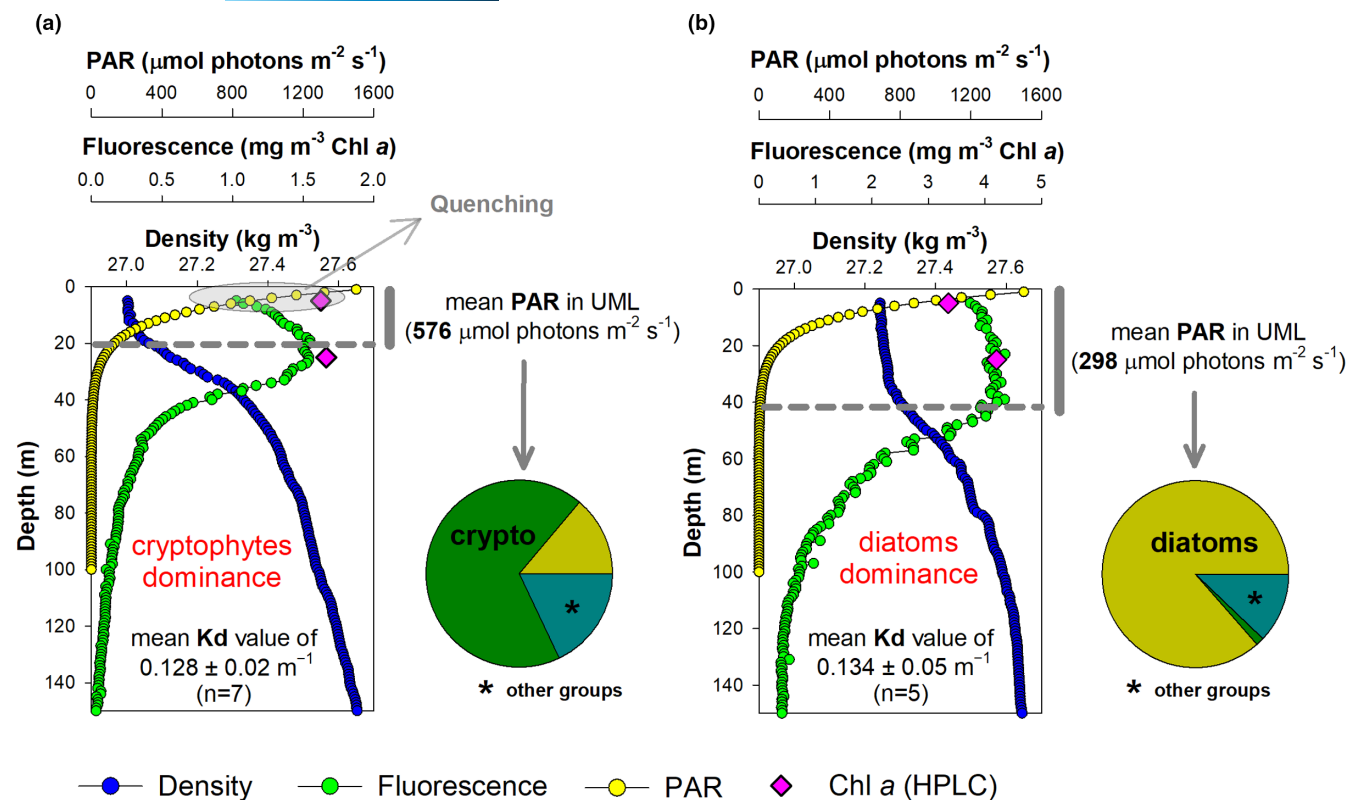
FIGURE 6 Typical vertical profiles of oceanographic properties in stations dominated by cryptophytes or diatoms. Mean vertical profiles of density, fluorescence (note the different magnitude range), and photosynthetically active radiation (PAR) of (a) seven selected cryptophytes-dominated (>60% of total chlorophyll *a*—Chl *a*) stations and (b) five selected diatoms-dominated (>75% of total Chl *a*) stations. The mean values of the upper mixed layer depth (gray horizontal dashed lines), as well as respective both mean PAR and attenuation coefficient (Kd) values in the upper mixed layer (UML), are also indicated. Additionally, the Chl *a* values determined by high performance liquid chromatography are also plotted for the samples collected within the UML of the selected stations, with which it is possible to observe a clear non-photochemical quenching (an upregulation of heat dissipation that will quench the Chl *a* fluorescence signal) associated with shallow mixed layers dominated by cryptophytes. See Section 2 for more details about the stations selection criteria. [Colour figure can be viewed at wileyonlinelibrary.com]

Tavano, Dotto, et al., 2018; Mendes, Tavano, Kerr, et al., 2018). The corresponding average PAR in the mixed layer (for a nominal clear-sky day in January/February, considering the maximum daily average peak of 1500 μmol photons m^{-2} s^{-1}, and with PAR attenuation calculated as the linear slope between depth and the natural logarithm of the measured downwelling PAR) was 576 μmol photons m^{-2} s^{-1} for the stations dominated by cryptophytes, decreasing to 298 μmol photons m^{-2} s^{-1} for the diatom-dominated stations (Figure 6). Presumably, the transitions (cycles) between LL and HL regimes in a shallow mixed layer are much faster than in deep mixing layers, requiring a fast capability of phytoplankton for photoadaptation, which may be favoring the cryptophytes in relation to the diatom's development across the NAP coastal waters.

Phytoplankton has evolutionarily developed a diverse set of physiological tools to survive in a highly variable environment. Photoregulation is an essential component of this plasticity, permitting the optimization of cell activities when faced with changing irradiance (Petrou et al., 2016). This is a challenge issue in phytoplankton ecology that certainly plays a key role on niche separation between diatoms and cryptophytes in the NAP. To the best of our knowledge, no joined experimental and field investigations are available in the

WAP concerning the response of marine phytoplankton assemblages under varying light conditions. However, in other Antarctic coastal areas, particularly in the Ross Sea, ambient light has been hypothesized as one of the key drivers of seasonal shifts in phytoplankton community composition, namely between *P. antarctica* and diatoms (Arrigo et al., 1999; Kropuenske et al., 2009). Although both diatoms and *P. antarctica* display very effective xanthophyll cycling (Alderkamp et al., 2010; van Leeuwe & Stefels, 2007), diatoms experience growth reduction under dynamic light conditions due to metabolic deficiencies linked with a poor photophysiological flexibility (Kropuenske et al., 2010; van Leeuwe et al., 2005); and this poses a serious trade-off to their lower iron requirements (Alderkamp et al., 2010). Phytoplankton organisms from the Ross Sea have evolved an iron-saving strategy whereby they photo-acclimate to LL by increasing their photosynthetic unit size rather than the number of their photosynthetic units, even when iron is available (Alderkamp et al., 2019). This adaptative strategy limits the growth of phytoplankton cells under fluctuating irradiance levels due to photodamage incurred during the high irradiance portion of the vertical mixing cycle (Alderkamp et al., 2010). Furthermore, D1—a protein that constitutes the core of the PSII reaction center—repair

rates are consistently too low to keep up with photodamage in the fluctuating light environments (Alderkamp et al., 2010). In shallow mixing layers, where irradiance fluctuations occur over very short time scales compared with relatively deeper mixing layers, all these processes could be intensified, possibly limiting the establishment and growth of certain diatom species (van de Poll et al., 2005; van Leeuwe et al., 2005).

Diatoms constitute a diversified group of species along the NAP, including centric and pennate forms (Costa et al., 2022). As such, it is unlikely that shallower mixing layers could be preventing all diatom species to grow and, consequently, accumulating biomass, especially those of pennate shapes that show high plasticity to cope with excess light (Petrou et al., 2016). However, based on our 11-year in-situ dataset, diatoms normally accumulate high biomass in relatively deep mixing layers, indicating a contrasting preferential fundamental niche to that observed for cryptophytes along the NAP (Figure S2; Costa et al., 2021). Future studies will be needed, and a better knowledge on the effects of irradiance on the photosynthetic physiology of both pennate and centric diatom forms occurring in the region is highly desirable for comparing their ecophysiological responses. Only then it will be possible to clarify the preferential distribution of diatoms in relatively deeper mixing layers and their very limited growth under confined shallow conditions associated with glacier meltwater input.

4 | CONCLUSION

Here, we showed that the recurrent biomass accumulation and dominance of cryptophytes in the NAP region can be attributed to their unique abilities to thrive under rapid and large fluctuations in light intensity, which are normally found in confined stratified upper mixed layers associated with glacial meltwater runoff. Due to increasing meltwater input processes associated with regional climate change, it is predicted that the upper mixed layer will become shallower, leading to a progressive increase in the averaged daily irradiance available to phytoplankton in surface waters. Thus, phytoplankton will be expected to be more exposed to light stress in the upper increasingly shallower layers, which presumably would present a favorable fundamental niche to the development of cryptophytes, potentially leading to an increase in the overall abundance and biomass of these nanoflagellates. This would cause significant ecological implications in the climate change-impacted fragile ecosystem of the NAP, with a potential impact in the krill stocks, which can threaten all Antarctic marine wildlife, from penguins to whales.

AUTHOR CONTRIBUTIONS
Carlos Rafael Borges Mendes and Raul Rodrigo Costa conceived this study. Carlos Rafael Borges Mendes wrote the first draft of the manuscript, with input from all authors, especially Raul Rodrigo Costa, Afonso Ferreira and Bruno Jesus. Carlos Rafael Borges Mendes, Raul Rodrigo Costa, Afonso Ferreira and Bruno Jesus designed the figures. Carlos Rafael Borges Mendes, Raul Rodrigo Costa and Miguel Costa Leal carried out the HPLC/CHEMTAX analyzes. Afonso Ferreira and Tiago Segabinazzi Dotto performed the remote sensing and physical analyzes, respectively. Carlos Rafael Borges Mendes, Bruno Jesus and Carolina Antuarte Islabão conducted the experiments and analyzed results. Carolina Antuarte Islabão and Andréa de Oliveira da Rocha Franco conducted the molecular and morphological phylogenetic analysis. Virginia Maria Tavano, Tiago Segabinazzi Dotto, Miguel Costa Leal, Rodrigo Kerr, Carolina Antuarte Islabão, Andréa de Oliveira da Rocha Franco, Mauricio M. Mata, Carlos Alberto Eiras Garcia and Eduardo Resende Secchi contributed to the organization and writing of the final version of the manuscript. All authors contributed to manuscript revision, read and approved the submitted version.

CONFLICT OF INTEREST STATEMENT

All authors declare they have no conflict of interests.

DATA AVAILABILITY STATEMENT

All data in the paper are present in the paper and the supplementary materials. The dataset contains the results of relative and absolute contributions of cryptophytes derived from the HPLC/CHEMTAX analysis are fully available at https://doi.org/10.5281/zenodo.5770533. The hydrographic dataset is available at Dotto et al. (2021). All other complementary data, already used in other publications (Table S1), are available at https://doi.org/10.5281/zenodo.5592163.

ORCID

Carlos Rafael Borges Mendes 🔟 https://orcid.org/0000-0001-6875-8860

Raul Rodrigo Costa 🔟 https://orcid.org/0000-0002-0940-3565

Afonso Ferreira 🔟 https://orcid.org/0000-0002-2670-8125

Bruno Jesus 🔟 https://orcid.org/0000-0002-2047-3783

Virginia Maria Tavano 🔟 https://orcid.org/0000-0003-0039-8111

Tiago Segabinazzi Dotto 🔟 https://orcid.org/0000-0003-0565-6941

Miguel Costa Leal 🔟 https://orcid.org/0000-0003-0672-6251

Rodrigo Kerr 🔟 https://orcid.org/0000-0002-2632-3137

Carolina Antuarte Islabão 🔟 https://orcid.org/0000-0001-5216-6553

Andréa de Oliveira da Rocha Franco 🔟 https://orcid.org/0000-0002-6656-8358

Mauricio M. Mata 🔟 https://orcid.org/0000-0002-9028-8284

Carlos Alberto Eiras Garcia 🔟 https://orcid.org/0000-0002-7629-4741

Eduardo Resende Secchi 🔟 https://orcid.org/0000-0001-9087-9909

REFERENCES

Akaike, H. (1974). A new look at the statistical model identification. *IEEE Transactions on Automatic Control*, 19, 716–723.

Alderkamp, A. C., Baar, H. J. W., Visser, R. J. W., & Arrigo, K. R. (2010). Can photoinhibition control phytoplankton abundance in deeply mixed water columns of the Southern Ocean? *Limnology and Oceanography*, 55, 1248–1264.

Alderkamp, A. C., van Dijken, G., Lowry, K. E., Lewis, K. M., Joy-Warren H., L., de Poll, W., Laan, P., Gerringa, L., Delmont, T. O., Jenkins, B., & Arrigo, K. R. (2019). Effects of iron and light availability on phytoplankton photosynthetic properties in the Ross Sea. *Marine Ecology Progress Series*, 621, 33–50.

Annett, A. L., Skiba, M., Henley, S., Venables, H. J., Meredith, M. P., Statham, P., & Ganeshram, R. (2015). Comparative roles of upwelling and glacial iron sources in Ryder Bay, coastal western Antarctic Peninsula. *Marine Chemistry*, 176, 21–33.

Araujo, M. L. V., Mendes, C. R. B., Tavano, V. M., Garcia, C. A. E., & Baringer, M. O. N. (2017). Contrasting patterns of phytoplankton pigments and chemotaxonomic groups along 30°S in the subtropical South Atlantic Ocean. *Deep Sea Research Part I: Oceanographic Reseach Papers*, 120, 112–121.

Armbrust, E. V. (2009). The life of diatoms in the world's oceans. *Nature*, 459, 185–192.

Arrigo, K. R., Robinson, D. H., Worthen, D. L., Dunbar, R. B., DiTullio, G. R., VanWoert, M., & Lizotte, M. P. (1999). Phytoplankton community structure and the drawdown of nutrients and CO_2 in the Southern Ocean. *Science*, 283, 365–367.

Bahlai, C. A., Hart, C., Kavanaugh, M. T., White, J. D., Ruess, R. W., Brinkman, T. J., Ducklow, H. W., Foster, D. R., Fraser, W. R., Genet, H., Groffman, P. M., Hamilton, S. K., Johnstone, J. F., Kielland, K., Landis, D. A., Mack, M. C., Sarnelle, O., & Thompson, J. R. (2021). Cascading effects: Insights from the U.S. long term ecological research network. *Ecosphere*, 12(5), e03430.

Beer, S., & Eshel, A. (1985). Determining phycoerythrin and phycocyanin concentrations in aqueous crude extracts of red algae. *Australian Journal of Marine and Freshwater Research*, 36, 785–792.

Bergmann, T., Fahnenstiel, G., Lohrenz, S., Millie, D., & Schofield, O. (2004). Impacts of a recurrent resuspension event and variable phytoplankton community composition on remote sensing reflectance. *Journal of Geophysical Research*, 109, C10S15.

Brown, M. S., Bowman, J. S., Lin, Y., Feehan, C. J., Moreno, C. M., Cassar, N., Marchetti, A., & Schofield, O. M. (2021). Low diversity of a key phytoplankton group along the West Antarctic Peninsula. *Limnology and Oceanography*, 66, 2470–2080.

Brown, M. S., Munro, D. R., Feehan, C. J., Sweeney, C., Ducklow, H. W., & Schofield, O. M. (2019). Enhanced oceanic CO_2 uptake along the rapidly changing West Antarctic Peninsula. *Nature Climate Change*, 9, 678–683.

Burki, F., Roger, A. J., Brown, M. W., & Simpson, A. G. B. (2020). The new tree of eukaryotes. *Trends in Ecology & Evolution*, 35, 43–55.

Campbell, J. W., & Aarup, T. (1989). Photosynthetically available radiation at high latitudes. *Limnology and Oceanography*, 34, 1490–1499.

Castro, C. G., Ríos, A. F., Doval, M. D., & Perez, F. F. (2002). Nutrient utilization and chlorophyll distribution in the Atlantic sector of the Southern Ocean during Austral summer 1995–96. *Deep Sea Research Part II: Topical Studies in Oceanography*, 49(4–5), 623–641.

Cerino, F., & Zingone, A. (2006). A survey of cryptomonad diversity and seasonality at a coastal Mediterranean site. *European Journal of Phycology*, 41, 363–378.

Claustre, H., Moline, M. A., & Prézelin, B. B. (1997). Sources of variability in the column photosynthetic cross section for Antarctic coastal waters. *Journal of Geophysical Research*, 102, 25047–25060.

Clem, K. R., Fogt, R. L., Turner, J., Lintner, B. R., Marshall, G. J., Miller, J. R., & Renwick, J. A. (2020). Record warming at the South Pole during the past three decades. *Nature Climate Change*, 10, 762–770.

Coelho, H., Cartaxana, P., Brotas, V., Queiroga, H., & Serôdio, J. (2011). Pheophorbide a in *Hydrobia ulvae* faecal pellets as a measure of microphytobenthos ingestion: Variation over season and period of day. *Aquatic Biology*, 13, 119–126.

Collini, E., Wong, C. Y., Wilk, K. E., Curmi, P. M. G., Brumer, P., & Scholes, G. D. (2010). Coherently wired light-harvesting on photosynthetic marine algae at ambient temperature. *Nature*, 463, 644–648.

Cook, A. J., Fox, A. J., Vaughan, D. G., & Ferrigno, J. G. (2005). Retreating glacier fronts on the Antarctic Peninsula over the past half-century. *Science*, 308, 541–544.

Cook, A. J., Holland, P. R., Meredith, M. P., Murray, T., Luckman, A., & Vaughan, D. G. (2016). Ocean forcing of glacier retreat in the western Antarctic Peninsula. *Science*, 353, 283–286.

Costa, R. R., Mendes, C. R. B., Ferreira, A., Tavano, V. M., Dotto, T. S., & Secchi, E. R. (2021). Large diatom bloom off the Antarctic Peninsula during cool conditions associated with the 2015/2016 El Niño. *Communications Earth & Environment*, 2, 252.

Costa, R. R., Mendes, C. R. B., Souza, M. S., Tavano, V. M., & Secchi, E. R. (2022). Chemotaxonomic characterization of the key genera of diatoms in the northern Antarctic Peninsula. *Anais da Academia Brasileira de Ciências*, 94(Suppl 1), e20210584.

Costa, R. R., Mendes, C. R. B., Tavano, V. M., Dotto, T. S., Kerr, R., Monteiro, T., Odebrecht, C., & Secchi, E. R. (2020). Dynamics of an intense diatom bloom in the northern Antarctic Peninsula, February 2016. *Limnology and Oceanography*, 65, 2056–2075.

Cunningham, B. R., Greenwold, M. J., Lachenmyer, E. M., Heidenreich, K. M., Davis, A. C., Dudycha, J. L., & Richardson, T. L. (2019). Light capture and pigment diversity in marine and freshwater cryptophytes. *Journal of Phycology*, 55, 552–564.

Darriba, D., Taboada, G. L., Doallo, R., & Posada, D. (2012). jModelTest 2: More models, new heuristics and parallel computing. *Nature Methods*, 9, 772.

Daugbjerg, N., Norlin, A., & Lovejoy, C. (2018). *Baffinella frigidus* gen. et sp. nov. (Baffinellaceae fam. nov., Cryptophyceae) from Baffin Bay: Morphology, pigment profile, phylogeny, and growth rate response to three abiotic factors. *Journal of Phycology*, 54, 665–680.

Davis, P., & Sieburth, J. (1984). Estuarine and oceanic microflagellate predation of actively growing bacteria: Estimation by frequency of dividing-divided bacteria. *Marine Ecology Progress Series*, 19, 237–246.

de Boyer Montégut, C., Madec, G., Fischer, A. S., Lazar, A., & Iudicone, D. (2004). Mixed layer depth over the global ocean: An examination of profile data and a profile-based climatology. *Journal of Geophysical Research*, 109, C12003.

Deane, A. J., Strachan, I. M., Saunders, G. W., Hill, D. R. A., & McFadden, G. I. (2002). Cryptomonad evolution: Nuclear 18S rDNA phylogeny versus cell morphology and pigmentation. *Journal of Phycology*, 38, 1236–1244.

Dierssen, H. M., Smith, R. C., & Vernet, M. (2002). Glacial meltwater dynamics in coastal waters west of the Antarctic peninsula. *Proceedings of the National Academy of Sciences of the United States of America*, 99, 1790–1795.

Dotto, T. S., Mata, M. M., Kerr, R., & Garcia, C. A. E. (2021). A novel hydrographic gridded data set for the northern Antarctic Peninsula. *Earth System Science Data*, 13, 671–696.

Ducklow, H. W., Baker, K., Martinson, D. G., Quetin, L. B., Ross, R. M., Smith, R. C., Stammerjohn, S. E., Vernet, M., & Fraser, W. (2007). Marine pelagic ecosystems: The West Antarctic Peninsula. *Philosophical Transactions of the Royal Society B*, 362, 67–94.

Ducklow, H. W., Fraser, W. R., Meredith, M. P., Stammerjohn, S. E., Doney, S. C., Martinson, D. G., Sailley, S. F., Schofield, O. M., Steinberg, D. K., Venables, H. J., & Amsler, C. D. (2013). West Antarctic Peninsula: An ice-dependent coastal marine ecosystem in transition. *Oceanography*, 26, 190–203.

Eilers, P. H. C., & Peeters, J. C. H. (1988). A model for the relationship between light intensity and the rate of photosynthesis in phytoplankton. *Ecological Modelling*, 42, 199–215.

Emden, K. H., Marin, B., & Melkoiam, M. (2002). Nuclear and nucleomorph SSU rDNA phylogeny in the Cryptophyta and the evolution of Cryptophyte diversity. *Journal of Molecular Evolution*, 55, 161–179.

Falkowski, P. G., Barber, R. T., & Smetacek, V. (1998). Biogeochemical controls and feedbacks on ocean primary production. *Science*, 281, 200–206.

Ferreira, A., Costa, R. R., Dotto, T. S., Kerr, R., Tavano, V. M., Brito, A. C., Brotas, V., Secchi, E. R., & Mendes, C. R. B. (2020). Changes in phytoplankton communities along the northern Antarctic Peninsula: Causes, impacts and research priorities. *Frontiers in Marine Science*, 7, 576254.

Forcada, J., Trathan, P. N., Reid, K., Murphy, E. J., & Croxall, J. P. (2006). Contrasting population changes in sympatric penguin species in association with climate warming. *Global Change Biology*, 12, 411–423.

Funk, C., Alami, M., Tibiletti, T., & Green, B. R. (2011). High light stress and the one-helix LHC-like proteins of the cryptophyte *Guillardia theta*. *Biochimica et Biophysica Acta*, 1807, 841–846.

Garibotti, I. A., Vernet, M., Kozlowski, A., & Ferrario, M. E. (2003). Composition and biomass of phytoplankton assemblages in coastal Antarctic water: A comparison of chemotaxonomic and microscopic analyses. *Marine Ecology Progress Series*, 247, 27–42.

Good, S., Fiedler, E., Mao, C., Martin, M. J., Maycock, A., Reid, R., Roberts-Jones, J., Searle, T., Waters, J., While, J., & Worsfold, M. (2020). The current configuration of the OSTIA system for operational production of foundation sea surface temperature and ice concentration analyses. *Remote Sensing*, 12, 720.

Guillard, R. R. L., & Hargraves, P. E. (1993). *Stichochrysis immobilis* is a diatom, not a chrysophyte. *Phycology*, 32, 234–236.

Harrop, S. J., Wilk, K. E., Dinshaw, R., Collini, E., Mirkovic, T., Teng, C. Y., Oblinsky, D. G., Green, B. R., Hoef-Emden, K., Hiller, R. G., Scholes, G. D., & Curmi, P. M. G. (2014). Single residue insertion switches the quaternary structure and exciton states of cryptophyte light harvesting proteins. *Proceedings of the National Academy of Sciences of the United States of America*, 111, E2666–E2675.

Henley, S. F., Schofield, O. M., Hendry, K. R., Schloss, I. R., Steinberg, D. K., Moffat, C., Peck, L. S., Costa, D. P., Bakker, D. C. E., Hughes, C., Rozema, P. D., Ducklow, H. W., Abele, D., Stefels, J., van Leeuwe, M. A., Brussaard, C. P. D., Buma, A. G. J., Kohut, J., Sahade, R., ... Meredith, M. P. (2019). Variability and change in the West Antarctic Peninsula marine system: Research priorities and opportunities. *Progress in Oceanography*, 173, 208–237.

Higashi, Y., & Seki, H. (2000). Ecological adaptation and acclimatization of natural freshwater phytoplankters with a nutrient gradient. *Environmental Pollution*, 109, 311–320.

Higgins, H. W., Wright, S. W., & Schlüter, L. (2011). Quantitative interpretation of chemotaxonomic pigment data. In S. Roy, C. A. Llewellyn, E. S. Egeland, & G. Johnson (Eds.), *Phytoplankton pigments: Characterization, chemotaxonomy and applications in oceanography* (pp. 257–313). Cambridge University Press.

Hill, D. R. A. (1991). A revised circumscription of *Cryptomonas* (Cryptopbyceae) based on examination of Australian strains. *Phycologia*, 30, 170–188.

Hill, D. R. A., & Rowan, K. S. (1989). The biliproteins of the cryptophyceae. *Phycologia*, 28, 455–463.

Höfer, J., Giesecke, R., Hopwood, M. J., Carrera, V., Alarcón, E., & González, H. E. (2019). The role of water column stability and wind mixing in the production/export dynamics of two bays in the western Antarctic Peninsula. *Progress in Oceanography*, 174, 105–116.

Hooker, S. B., Van Heukelem, L., Thomas, C. S., Claustre, H., Ras, J., Barlow, R., Sessions, H., Schlüter, L., Perl, J., Trees, C., Stuart, V., Head, E., Clementson, L., Fishwick, J., Llewellyn, C., & Aiken, J. (2005). *The Second Sea-WiFS HPLC Analysis Round-Robin Experiment (SeaHARRE-2)*. NASA Goddard Space Flight Center.

Huot, Y., Babin, M., Bruyant, F., Grob, C., Twardowski, M. S., & Claustre, H. (2007). Relationship between photosynthetic parameters and different proxies of phytoplankton biomass in the subtropical ocean. *Biogeosciences*, 4, 853–868.

Ilmavirta, V. (1988). Phytoflagellates and their ecology in Finnish brown water lakes. *Hydrobiologia*, 161, 255–270.

Jeffrey, S. W. (1974). Profiles of photosynthetic pigments in the ocean using thin-layer chromatography. *Marine Biology*, 26, 101–110.

Jeffrey, S. W., Mantoura, R. F. C., & Wright, S. W. (1997). *Phytoplankton pigments in oceanography: Guidelines to modern Methods*. UNESCO.

Joy-Warren, H., van Dijken, G. L., Alderkamp, A.-C., Leventer, A., Lewis, K. M., Selz, V., Lowry, K. E., van de Poll, W., & Arrigo, K. R. (2019). Light is the primary driver of early season phytoplankton production along the western Antarctic Peninsula. *Journal of Geophysical Research-Oceans*, 124, 7375–7399.

Kaňa, R., Kotabová, E., Sobotka, R., & Prášil, O. (2012). Non-photochemical quenching in cryptophyte alga *Rhodomonas salina* in located in chlorophyll a/c antennae. *PLoS One*, 7, e29700.

Kerr, R., Mata, M. M., Mendes, C. R. B., & Secchi, E. R. (2018). Northern Antarctic Peninsula: A marine climate hotspot of rapid changes on ecosystems and ocean dynamics. *Deep Sea Research Part II: Topical Studies in Oceanography*, 149, 4–9.

Kim, H., Doney, S. C., Iannuzzi, R. A., Meredith, M. P., Martinson, D. G., & Ducklow, H. W. (2016). Climate forcing for dynamics of dissolved inorganic nutrients at Palmer Station, Antarctica: An interdecadal (1993–2013) analysis. *Journal of Geophysical Research: Biogeosciences*, 121, 2369–2389.

Kropuenske, L. R., Mills, M. M., van Dijken, G. L., Alderkamp, A. C., Mine Berg, G., Robinson, D. H., Welschmeyer, N. A., & Arrigo, K. R. (2010). Strategies and rates of photoacclimation in two major Southern Ocean phytoplankton taxa: *Phaeocystis antarctica* (Haptophyta) and *Fragilariopsis cylindrus* (Bacillariophyceae). *Journal of Phycology*, 46, 1138–1151.

Kropuenske, L. R., Mills, M. M., van Dijken, G. L., Bailey, S., Robinson, D. H., Welschmeyer, N. A., & Arrigoa, K. R. (2009). Photophysiology in two major Southern Ocean phytoplankton taxa: Photoprotection in *Phaeocystis antarctica* and *Fragilariopsis cylindrus*. *Limnology and Oceanography*, 54, 1176–1196.

Kumar, S., Stecher, G., Li, M., Knyaz, C., & Tamura, K. (2018). MEGA X: Molecular Evolutionary Genetics Analysis across computing platforms. *Molecular Biology and Evolution*, 35, 1547–1549.

Laviale, M., & Neveux, J. (2011). Relationships between pigment ratios and growth irradiance in 11 marine phytoplankton species. *Marine Ecology Progress Series*, 425, 63–77.

Laza-Martínez, A. (2012). *Urgorri complanatus* gen. et. sp. nov. (Cryptophyceae), a red-tide-forming specie in brackish waters. *Journal of Phycology*, 48, 423–435.

Mackey, D. J., Higgins, H. W., Mackey, M. D., & Holdsworth, D. (1998). Algal class abundances in the western equatorial pacific: Estimation from HPLC measurements of chloroplast pigments using CHEMTAX. *Deep-Sea Research Part I: Oceanographic Research Papers*, 45, 1441–1468.

Mackey, M. D., Mackey, D. J., Higgins, H. W., & Wright, S. W. (1996). CHEMTAX – A program for estimating class abundances from chemical markers: Application to HPLC measurements of phytoplankton. *Marine Ecology Progress Series*, 144, 265–283.

Madeira, F., Park, Y., Lee, J., Buso, N., Gur, T., Madhusoodanan, N., Basutkar, P., Tivey, A. R. N., Potter, S. C., Finn, R. D., & Lopez, R. (2019). The EMBL-EBI search and sequence analysis tools APIs in 2019. *Nucleic Acids Research*, 47, W636–W641.

Marin, B., Klingberg, M., & Melkonian, M. (1998). Phylogenetic relationships among the Cryptophyta: Analyses of nuclear-encoded SSU rRNA sequences support the monophyly of extant plastid-containing lineages. *Protist*, 149, 265–276.

McDougall, T. J., & Barker, P. M. (2011). *Getting started with TEOS-10 and the Gibbs Seawater (GSW) Oceanographic Toolbox (SCOR/IAPSO WG127)*.

Mendes, C. R., Cartaxana, P., & Brotas, V. (2007). HPLC determination of phytoplankton and microphytobenthos pigments: Comparing resolution and sensitivity of a C18 and a C8 method. *Limnology and Oceanography: Methods*, 5, 363–370.

Mendes, C. R. B., de Souza, M. S., Garcia, V. M. T., Leal, M. C., Brotas, V., & Garcia, C. A. E. (2012). Dynamics of phytoplankton communities during late summer around the tip of the Antarctic Peninsula. *Deep Sea Research Part I: Oceanographic Reseach Papers*, 65, 1–14.

Mendes, C. R. B., Kerr, R., Tavano, V. M., Cavalheiro, F. A., Garcia, C. A. E., Dessai, D. R. G., & Anilkumar, N. (2015). Cross-front phytoplankton pigments and chemotaxonomic groups in the Indian sector of the Southern Ocean. *Deep Sea Research Part II: Topical Studies in Oceanography*, 118, 221–232.

Mendes, C. R. B., Tavano, V. M., Dotto, T. S., Kerr, R., de Souza, M. S., Garcia, C. A. E., & Secchi, E. R. (2018). New insights on the dominance of cryptophytes in Antarctic coastal waters: A case study in Gerlache Strait. *Deep-Sea Research Part II: Topical Studies in Oceanography*, 149, 161–170.

Mendes, C. R. B., Tavano, V. M., Kerr, R., Dotto, T. S., Maximiano, T., & Secchi, E. R. (2018). Impact of sea ice on the structure of phytoplankton communities in the northern Antarctic Peninsula. *Deep-Sea Research Part II: Topical Studies in Oceanography*, 149, 111–123.

Mendes, C. R. B., Tavano, V. M., Leal, M. C., de Souza, M. S., Brotas, V., & Garcia, C. A. E. (2013). Shifts in the dominance between diatoms and cryptophytes during three late summers in the Bransfield Strait (Antarctic Peninsula). *Polar Biology*, 36, 537–547.

Meredith, M. P., Stammerjohn, S. E., Ducklow, H. W., Leng, M. J., Arrowsmith, C., Brearley, J. A., Venables, H. J., Barham, M., van Wessem, J. M., Schofield, O., & Waite, N. (2021). Local- and large-scale drivers of variability in the coastal freshwater budget of the Western Antarctic Peninsula. *Journal of Geophysical Research: Oceans*, 126, e2021JC017172. https://doi.org/10.1029/2021JC017172

Moline, M. A., Claustre, H., Frazer, T. K., Schofield, O., & Vernet, M. (2004). Alteration of the food web along the Antarctic Peninsula in response to a regional warming trend. *Global Change Biology*, 10, 1973–1980.

Montes-Hugo, M., Doney, S. C., Ducklow, H. W., Fraser, W., Martinson, D., Stammerjohn, S. E., & Schofield, O. (2009). Recent changes in phytoplankton communities associated with rapid regional climate change along the western Antarctic Peninsula. *Science*, 323, 1470–1473.

Mora, S., Whitehead, R., & Gregory, M. (1994). The chemical composition of glacial melt water ponds and streams on the McMurdo Ice Shelf, Antarctica. *Antarctic Science*, 6(1), 17–27.

Moreau, S., Ferreyra, G. A., Mercier, B., Lemarchand, K., Lionard, M., Roy, S., Mostajir, B., Roy, S., van Hardenberg, B., & Demers, S. (2010). Variability of the microbial community in the western Antarctic Peninsula from late fall to spring during a low ice cover year. *Polar Biology*, 33, 1599–1614.

Nei, M., & Kumar, S. (2000). *Molecular evolution and phylogenetics*. Oxford University Press.

Novarino, G. (2003). A companion to the identification of cryptomonad flagellates (Cryptophyceae = Cryptomonadea). *Hydrobiologia*, 502, 225–270.

Nowacek, D. P., Friedlaender, A. S., Halpin, P. N., Hazen, E. L., Johnston, D. W., Read, A. J., Espinasse, B., Zhou, M., & Zhu, Y. (2011). Super-aggregations of krill and humpback whales in Wilhelmina Bay, Antarctic Peninsula. *PLoS One*, 6, e19173.

Oliva, M., Navarro, F., Hrbáček, F., Hernández, A., Nývlt, D., Pereira, P., Ruiz-Fernández, J., & Trigo, R. (2017). Recent regional climate cooling on the Antarctic Peninsula and associated impacts on the cryosphere. *Science of the Total Environment*, 580, 210–223.

Pan, B. J., Vernet, M., Manck, L., Forsch, K., Ekern, L., Mascioni, M., Barbeau, K. A., Almandoz, G. O., & Orona, A. J. (2020). Environmental drivers of phytoplankton taxonomic composition in an Antarctic fjord. *Progress in Oceanography*, 183, 102295.

Paolo, F. S., Fricker, H. A., & Padman, L. (2015). Volume loss from Antarctic ice shelves is accelerating. *Science*, 348, 327–331.

Petrou, K., Kranz, S. A., Trimborn, S., Hassler, C. S., Ameijeiras, S. B., Sackett, O., Ralph, P. J., & Davidson, A. T. (2016). Southern Ocean phytoplankton physiology in a changing climate. *Journal of Plant Physiology*, 203, 135–150.

Pinckney, J., Paerl, H., Harrington, M., & Howe, K. (1998). Annual cycles of phytoplankton community-structure and bloom dynamics in the Neuse River Estuary, NC. *Marine Biology*, 131, 371–381.

Pondaven, P., Ragueneau, O., Tréguer, P., Hauvespre, A., Dezileau, L., & Reyss, J. L. (2000). Resolving the "opal paradox" in the Southern Ocean. *Nature*, 405, 168–172.

Pritchard, H., Ligtenberg, S. R. M., Fricker, H. A., Vaughan, D. G., van den Broeke, M. R., & Padman, L. (2012). Antarctic ice-sheet loss driven by basal melting of ice shelves. *Nature*, 484, 502–505.

Ralph, P. J., & Gademann, R. (2005). Rapid light curves: A powerful tool to assess photosynthetic activity. *Aquatic Botany*, 82, 222–237.

Reize, I. B., & Melkonian, M. (1989). New way to investigate living flagellated kiliated cells in the light microscope: Immobilization of cells in agarose. *Botanica Acta*, 102, 145–151.

Rintoul, S. R. (2018). The global influence of localized dynamics in the Southern Ocean. *Nature*, 558, 209–218.

Rodriguez, F., Oliver, J. L., Marín, A., & Medina, J. R. (1990). The general stochastic model of nucleotide substitution. *Journal of Theoretical Biology*, 142, 485–501.

Ronquist, F., & Huelsenbeck, J. P. (2003). MrBayes 3: Bayesian phylogenetic inference under mixed models. *Bioinformatics*, 19, 1572–1574.

Rousseaux, C., & Gregg, W. (2014). Interannual variation in phytoplankton primary production at a global scale. *Remote Sensing*, 6, 1–19.

Roy, S., Llewellyn, C. A., Egeland, E. S., & Johnsen, G. (2011). *Phytoplankton pigments: Characterization, chemotaxonomy and applications in oceanography*. Cambridge University Press.

Rozema, P. D., Venables, H. J., van de Poll, W. H., Clarke, A., Meredith, M. P., & Buma, A. G. J. (2017). Interannual variability in phytoplankton biomass and species composition in northern Marguerite Bay (West Antarctic Peninsula) is governed by both winter sea ice cover and summer stratification. *Limnology and Oceanography*, 62, 235–252.

Saba, G. K., Fraser, W. R., Saba, V. S., Iannuzzi, R. A., Coleman, K. E., Doney, S. C., Ducklow, H. W., Martinson, D. G., Miles, T. N., Patterson-Fraser, D. L., Stammerjohn, S. E., Steinberg, D. K., & Schofield, O. M. (2014). Winter and spring controls on the summer food web of the coastal West Antarctic Peninsula. *Nature Communications*, 5, 4318.

Schlüter, L., Møhlenberg, F., Havskum, H., & Larsen, S. (2000). The use of phytoplankton pigments for identifying and quantifying phytoplankton groups in coastal areas: Testing the influence of light and nutrients on pigment/chlorophyll *a* ratios. *Marine Ecology Progress Series*, 192, 49–63.

Schofield, O., Ducklow, H. W., Martinson, D. G., Meredith, M. P., Moline, M. A., & Fraser, W. R. (2010). How do polar marine ecosystems respond to rapid climate change? *Science*, 328, 1520–1523.

Schofield, O., Saba, G., Coleman, K., Carvalho, F., Couto, N., Ducklow, H., Finkel, Z., Irwin, A., Kahl, A., Miles, T., Montes-Hugo, M., Stammerjohn, S., & Waite, N. (2017). Decadal variability in coastal phytoplankton community composition in a changing West Antarctic Peninsula. *Deep-Sea Research Part I: Oceanographic Research Papers*, 124, 42–54.

Schofield, O., Brown, M., Kohut, J., Nardelli, S., Saba, G., Waite, N., & Ducklow, H. (2018). Changes in the upper ocean mixed layer and phytoplankton productivity along the West Antarctic Peninsula. *Philosophical Transactions of the Royal Society A*, 376, 20170173.

Schreiber, U., Bilger, W., & Neubauer, C. (1994). Chlorophyll fluorescence as a non-intrusive indicator for rapid assessment of in vivo photosynthesis. In E. Schulze & M. Caldwell (Eds.), *Ecophysiology of photosynthesis* (pp. 49–70). Springer-Verlag.

Seyboth, E., Groch, K. R., Dalla Rosa, L., Reid, K., Flores, P. A. C., & Secchi, E. R. (2016). Southern right whale (*Eubalaena australis*) reproductive success is influenced by krill (*Euphausia superba*) density and climate. *Scientific Reports*, 6, 28205.

Shaw, T. J., Raiswell, R., Hexel, C. R., Vu, H. P., Moore, W. S., Dudgeon, R., & Smith, K. L., Jr. (2011). Input, composition, and potential impact of terrigenous material from free-drifting icebergs in the Weddell Sea. *Deep-Sea Research Part II: Topical Studies in Oceanography*, 58, 1376–1383.

Shuman, F. R., & Lorenzen, C. J. (1975). Quantitative degradation of chlorophyll by a marine herbivore. *Limnology and Oceanography*, 20, 580–586.

Stammerjohn, S. E., Martinson, D. G., Smith, R. C., Yuan, X., & Rind, D. (2008). Trends in Antarctic annual sea ice retreat and advance and their relation to El Niño–Southern oscillation and Southern Annular Mode variability. *Journal of Geophysical Research, Oceans*, 113, C03S90.

Stammerjohn, S. E., Massom, R., Rind, D., & Martinson, D. G. (2012). Regions of rapid sea ice change: An inter-hemispheric seasonal comparison. *Geophysical Research Letters*, 39, L06501.

Stammerjohn, S. E., & Scambos, T. A. (2020). Warming reaches the South Pole. *Nature Climate Change*, 10, 710–711.

Steig, E. J., Schneider, D. P., Rutherford, S. D., Mann, M. E., Comiso, J. C., & Shindell, D. T. (2009). Warming of the Antarctic ice-sheet surface since the 1957 International Geophysical Year. *Nature*, 457, 459–463.

Tamigneaux, E., Vazquez, E., Mingelbier, M., Kelein, B., & Legendre, L. (1995). Environmental control pf phytoplankton assemblages in nearshore marine waters, with special emphasis on phototrophic ultraplankton. *Journal of Plankton Research*, 17, 1421–1447.

Taylor, D. L., & Lee, C. C. (1971). A new cryptomonad from Antarctica: *Cryptomonas cryophila* sp. nov. *Archiv für Mikrobiologie*, 75, 269–280.

Thoisen, C., Hansen, B. W., & Nielsen, S. L. (2017). A simple and fast method for extraction and quantification of cryptophyte phycoerythrin. *MethodsX*, 4, 209–213.

Trefault, N., de la Iglesia, R., Moreno-Pino, M., dos Santos, A. L., Ribeiro, C. G., Parada-Pozo, G., Cristi, A., Marie, D., & Vaulot, D. (2021). Annual phytoplankton dynamics in coastal waters from Fildes Bay, western Antarctic Peninsula. *Scientific Reports*, 11, 1368.

Trivelpiece, W. Z., Hinke, J. T., Miller, A. K., Reiss, C. S., Trivelpiece, S. G., & Watters, G. M. (2011). Variability in krill biomass links harvesting and climate warming to penguin population changes in Antarctica. *Proceedings of the National Academy of Sciences of the United States of America*, 108, 7625–7628.

Turner, J., Colwell, S. R., Marshall, G. J., Lachlan-Cope, T. A., Carleton, A. M., Jones, P. D., Lagun, V., Reid, P. A., & Iagovkina, S. (2005). Antarctic climate change during the last 50 years. *International Journal of Climatology*, 25, 279–294.

Turner, J., Lu, H., White, I., King, J. C., Phillips, T., Hosking, J. S., Bracegirdle, T. J., Marshall, G. J., Mulvaney, R., & Deb, P. (2016). Absence of 21st century warming on Antarctic Peninsula consistent with natural variability. *Nature*, 535, 411–415.

van de Poll, W. H., van Leeuwe, M. A., Roggeveld, J., & Buma, A. G. J. (2005). Nutrient limitation and high irradiance acclimatation reduce PAR and UV-induced viability loss in the Antarctic diatom *Chaetoceros brevis* (Bacillariophyceae). *Journal of Phycology*, 41, 840–850.

van den Hoff, J., Bell, E., & Whittock, L. (2020). Dimorphism in the Antarctic cryptophyte *Geminigera cryophila* (Cryptophyceae). *Journal of Phycology*, 56, 1028–1038.

van Leeuwe, M. A., & Stefels, J. (2007). Photosynthetic responses in *Phaeocystis antarctica* towards varying light and iron conditions. *Biogeochemistry*, 83, 61–70.

van Leeuwe, M. A., van Sikkelerus, B., Gieskes, W. W. C., & Stefels, J. (2005). Taxon-specific differences in photoacclimation to fluctuating irradiances in an Antarctic diatom and a green flagellate. *Marine Ecology Progress Series*, 288, 9–19.

West, R., Keşan, G., Trsková, E., Sobotka, R., Kaňa, R., Fuciman, M., & Polívka, T. (2016). Spectroscopic properties of the triple bond carotenoid alloxanthin. *Chemical Physics Letters*, 653, 167–172.

Wood, A. M., Everroad, R. C., & Wingard, L. M. (2005). Measuring growth rates in microalgal cultures. In R. Andersen (Ed.), *Algal culturing techniques* (pp. 269–285). Elsevier Academic Press.

Wright, S. W., Ishikawa, A., Marchant, H. J., Davidson, A. T., van den Enden, R. L., & Nash, G. V. (2009). Composition and significance of picophytoplankton in Antarctic waters. *Polar Biology*, 32, 797–808.

Wright, S. W., van den Enden, R. L., Pearce, I., Davidson, A. T., Scott, F. J., & Westwood, K. J. (2010). Phytoplankton community structure and stocks in the Southern Ocean (30–80°E) determined by CHEMTAX analysis of HPLC pigment signatures. *Deep Sea Research Part II: Topical Studies in Oceanography*, 57, 758–778.

Zapata, M., Rodríguez, F., & Garrido, J. L. (2000). Separation of chlorophylls and carotenoids from marine phytoplankton: A new HPLC method using a reversed phase C8 column and pyridine-containing mobile phases. *Marine Ecology Progress Series, 195,* 29–45.

Zar, J. H. (1996). *Biostatistical analysis* (3rd ed.). Prentice Hall.

SUPPORTING INFORMATION

Additional supporting information can be found online in the Supporting Information section at the end of this article.